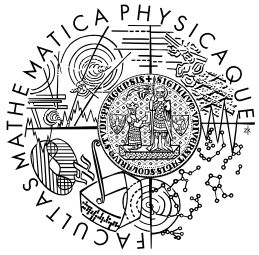

FACULTY
OF MATHEMATICS
AND PHYSICS
Charles University

BACHELOR THESIS

Marcel Štolc

Tidal disruption in the vicinity of black holes in active galaxies

Astronomical Institute of the Charles University in Prague

Supervisor of the bachelor thesis:	RNDr. Jiří Svoboda, Ph.D.
Study programme:	Physics
Study branch:	General Physics

Prague 2017

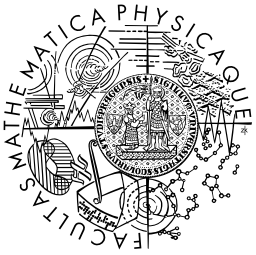

MATEMATICKO-FYZIKÁLNÍ FAKULTA
Univerzita Karlova

BAKALÁŘSKÁ PRÁCE

Marcel Štolc

Slapové trhání v blízkosti černých děr v aktivních galaxiích

Astronomický ústav Univerzity Karlovy v Praze

Vedoucí bakalářské práce: RNDr. Jiří Svoboda, Ph.D.

Studijní program: Fyzika

Studijní obor: Obecná fyzika

Praha 2017

I declare that I carried out this bachelor thesis independently, and only with the cited sources, literature and other professional sources.

I understand that my work relates to the rights and obligations under the Act No. 121/2000 Sb., the Copyright Act, as amended, in particular the fact that the Charles University has the right to conclude a license agreement on the use of this work as a school work pursuant to Section 60 subsection 1 of the Copyright Act.

In Prague, May 14, 2017

Title: Tidal disruption in the vicinity of black holes in active galaxies

Author: Marcel Štolc

Department: Astronomical Institute of the Charles University in Prague

Supervisor: RNDr. Jiří Svoboda, Ph.D., Astronomical Institute of the Czech Academy of Sciences

Abstract: In this thesis we studied tidal disruptions of stars in the vicinity of compact objects and performed spectral re-analysis of XMMSL1 J074008.2-853927, one of the most prominent candidates of tidal disruption events (TDE) around super-massive black holes. This particular TDE shows signs of thermal and non-thermal radiation component and is also indicating the energy excess corresponding to the iron line emission of Fe Kα line. We analysed X-ray spectra from two XMM-Newton observations - from the 30-th of April 2014 and the 12-th of January 2015 that were follow-up observations after the discovery of this TDE. We confirmed the possible thermal and non-thermal profile of radiation and the presence of Fe Kα line in the data of the first XMM-Newton follow-up observation. We studied in detail the parameters of the iron line, which cannot be to tightly constrained due to insufficient quality of data. However, we also showed that in case of modelling the excess in lower energy band with relativistic reflection the parameters can be constrained.

Keywords: black holes, tidal disruption, active galaxies

Název práce: Slapové trhání v blízkosti černých děr v aktivních galaxiích

Autor: Marcel Štolc

Katedra: Astronomický ústav Univerzity Karlovy v Praze

Vedoucí bakalářské práce: RNDr. Jiří Svoboda, Ph.D., Astronomický ústav Akademie věd České republiky

Abstrakt: V této práci jsme studovali slapové trhání hvězd v okolí kompaktních objektů a provedli spektrální re-analýzu XMMSL1 J074008.2-853927, jednoho z nejvýznamnějších kandidátů událostí slapového trhání (TDE) okolo super- masivních černých děr. Tato konkrétní TDE vykazuje znaky termální a netermální složky záření a zároveň naznačuje přebytek energie odpovídající emisi čáry železa Fe Kα. Analyzovali jsme rentgenové spektra ze dvou pozorování XMM-Newton - ze dne 30. dubna 2014 a 12. ledna 2015, které byly navazujícími pozorováními po objevení této TDE. Potvrdili jsme možný termální a netermální profil záření a přítomnost Fe Kα v datech z prvního navazujícího pozorování XMM-Newton. Podrobně jsme studovali parametry čáry železa, které nemohou být pevně omezeny kvůli nedostatečné kvalitě dat. Ukázalo se však také, že v případě modelování přebytku v nižším energetickém pásmu relativistickou reflekcí parametry možno omezit.

Klíčová slova: černé díry, slapové trhání, aktivní galaxie

My thanks goes to my supervisor, RNDr. Jiří Svoboda, Ph.D., for the opportunity to gain new knowledge, for the helpful advice and observations and all the time spent working on this thesis.

I would also like to express my gratitude to Dr. Richard Saxton for providing us data from XMM-Newton telescope and his helpful comments.

Contents

Preface

The tidal disruption occurs in case of a star (generally it could be any celestial object) wandering its way too close to the galactic centre, where it gets partially ripped apart. Afterwards the stellar debris are accreted onto the black hole while emitting luminous flares in the X-ray and UV spectra.
The first papers proposing a possible occurrence of such a phenomenon came from Hills [1975] and Rees [1988]. Shortly after that in the mid 90s the first candidates as a possible result of tidal disruption scenario were observed, e.g. the active galactic nucleus Zwicky 159.034 and its sudden rebrightening in the soft X-ray- and UV-bands (Brandt et al. [1995]).

The interest in these events has risen since then along with the quality of the observations. Thanks to the follow-up observations there are more data available, which help to improve the statistic of observations depending on the number of studied samples. They also help to ensure higher probability of success while testing the theory predictions and numerical models based on them.
However, current studies point out that the models capable of predicting the tidal disruptions are not yet finished. There are number of parameters that are taken into account, e.g. the type of disrupted star, trajectory of disrupted star, accretion disc and accretion wind evolution at latter stages of the tidal disruptions, etc. It's also due to the intrinsic character of the process, i.e. 3 dimensional hydrodynamic problem involving the emission, whose study is approached respectively.

The amount of tidal disruption candidates is showing signs of growth thanks to the current observations. This rising trend will be in the near future considered a powerful tool, which will help to establish the demographical distribution of black holes in the universe. Also the more tidal disruptions will be detected the sooner will be understood if there really is a justification for black hole differentiation to black holes, intermediate black holes and super-massive black holes (see Auchettl et al. [2017] and references therein).

It is widely believed that there is a chance that deeper study of these disruptive events could enable us to find the answers to dazzling questions regarding the nature of the jet formation and to determine the conditions that have to be met in order to create them. There are two such celestial events that could potentially shed a light on this particular matter, both suspected to launch jets: Swift J1644+57 (Cummings et al. [2011]) and Swift J2058+05 (Cenko et al. [2012]).
There's also been developed an interesting idea arguing that the extreme tidal disruptive encounters of celestial objects with a massive, compact one could explain the origin of gamma-ray burst and their variants.

Last but not least such events present themselves not only in the electromagnetic spectra. The partial distortion or engulfment of a whole star by the (supermassive) black hole should be accompanied by the shaking of the space-time fabric, i.e. gravitational waves. The possibility that in such cases the gravitational waves could be detectable is very low but the tidal disruption's traits,

especially the time evolution of bolometric luminosity, could be used to predict the gravitational waves of much higher magnitudes, in fact those caused by the recoiling (super-massive) black holes (Liu et al. [2009]).

1. Introduction

1.1 Black holes

The black holes (BHs hereafter) are results of gravitational collapse of a star, which runs out of fuel and is not capable of sustaining its form due to its own gravity. The name comes from the fact that nothing, not even light can escape from the area within the event horizon. These massive, compact objects can be characterised by set of three numbers: mass, spin and charge according to the No-hair theorem (Misner et al. [1973]).

The most massive BHs being called the super-massive black holes (SMBHs hereafter) are suspected to be lurking at the centre of each galaxy in the universe (Magorrian et al. [1998]). According to the presence of surrounding material SMBHs can be active on non-active. The active galactic nucleus (AGN hereafter) consists of SMBH and the accretion disc surrounding it (see e.g. Kazanas et al. [2012] and references therein). The material forming the accretion disc is orbiting the SMBH at such speed that it is emitting large amount of energy in the spectra. The counterpart of active galaxies are the inactive galaxies. Such galaxies are supposed to have a SMBH at its centre that is quiescent, i.e. it does not have an accretion disc around it.

BHs can be found not only in the centre of each galaxy (especially the super-massive ones), as stated above. They can also be a part of so called binary systems. Such systems consist of a donor component (usually a star) and an accretor component (neutron star or BH). These binary systems, called X-ray binaries (see Tauris and van den Heuvel [2006] and references therein), got their name because of the X-ray radiation emitted during the accretion.

1.2 Black hole accretion

When any matter gets in the vicinity of a compact massive object at some point its components start to wrap around it in slow spiralling motions in a process called accretion. The newly formed accretion disc, as a result of diffused material trying to conserve the non-zero angular momentum it had before the interaction with the compact massive object, usually consists of gas, dust or other constituents that can be found in the celestial debris. They are heated to high temperature due to the gravitational and frictional forces acting on them. These, circumstances under which the accretion of matter takes place lead to producing high energy flares in X-rays or gamma rays. The luminosity produced during the accretion is proportional to the accretion rate (see e.g. Alloin et al. [2006] and references therein). In the case of a possible tidal disruption scenario the accretion discs are signposts of momentary galactic activity onset but in contrast to the accretion discs in AGN they are eventually engulfed by the SMBH.

1.3 Effects of strong gravity

The radiation emerging in the close proximity of BH is affected by its gravity. The high-energy spectra - X-ray spectra can be used to study the profiles of certain emission lines. The strongest observed emission line is the iron Fe Kα line at 6.4 keV. The strength of the iron emission line is characterised by its equivalent width. The parameters that can affect the Fe Kα line are the metal abundances in the galactic centre, the inclination of accretion disc and the ionisation state of iron, which when fully ionised is characterised by the emission line energy 6.97 keV. The intrinsic trait of Fe Kα line is its narrow profile. The strong gravitation field together with the Doppler shift effect cause the Fe Kα line to broaden and skew, which can be studied in order to determine the inclination of accretion disc, constrain its size, the spin or the mass of SMBH harboured in the AGN (e.g Fabian et al. [1989]; Kojima [1991]; Dovčiak et al. [2004a]; etc.). The first clear broad spectral Fe Kα line in AGN was observed by Tanaka et al. [1995].

1.4 Tidal disruption

When a star of mass $M_{\rm star}$ and radius $R_{\rm star}$ gets on its orbit too close to the core of the galaxy, i.e. the SMBH, it can be tidally stripped. Such a scenario, called tidal disruption, is expected to be an inevitable consequence for a star on a parabolic-like orbit (with total zero energy) that reached the tidal radius $R_{\rm tidal}$ given as

$$R_{tidal} = \left(\frac{2M_{\rm SMBH}}{M_{\rm star}}\right)^{\frac{1}{2}} R_{\rm star}. \tag{1.1}$$

The idea standing behind the derivation of the equation 1.1 (Hills [1975]; Rees [1988]) is based on equality of gravitational self-force of the star, i.e. its self-gravity, and the tidal force due to the tremendous gravitational pull of SMBH. Reaching the tidal radius $R_{\rm tidal}$ does not necessarily mean that the star will be torn apart and swallowed whole by the SMBH.
The inverse impact factor β (Stone [2015]), a dimensionless quantity, given as

$$\beta = \frac{R_{\rm pericenter}}{R_{\rm tidal}} \tag{1.2}$$

describes the strength of tidal disruption depending on the trajectory of a studied star. The Figure 1.1 illustrates the dependence of spatial parameters of tidal disruption. The concept of so called cross sections of tidal disruption describes a partial mass stripping, wherein star loses a certain amount of its mass after the encounter with the BH depending on the trajectory of studied star and its nature (main-sequence star, white dwarf, etc.)

While the tidal radius is proportional to $M_{\rm SMBH}^{\frac{1}{3}}$, the Schwarzschild radius $R_{\rm g}$, defined as

$$R_{\rm g} = \frac{GM}{c^2}, \tag{1.3}$$

where G is gravitational constant, M object mass and c speed of light, is proportional to the SMBH's mass M_{SMBH} itself. This leads to the conclusion that there is a certain critical mass of SMBH, defined as

$$M_{\mathrm{Hills}} = 1.1 \times 10^8 M_\odot \left(\frac{R_{\mathrm{star}}}{R_\odot}\right)^{\frac{3}{2}} \left(\frac{M_{\mathrm{star}}}{M_\odot}\right)^{-\frac{1}{2}}, \tag{1.4}$$

above which the stars will be swallowed by the SMBH's event horizon before ever reaching the point of the tidal disruption scenario (Stone [2015]).

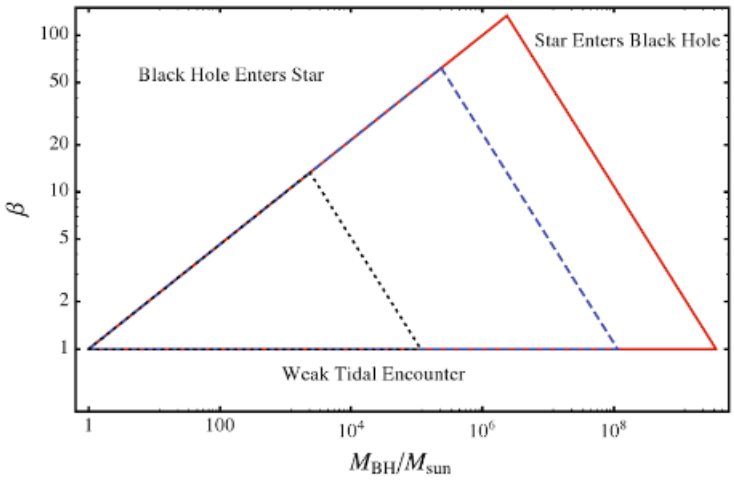

Figure 1.1: The dependence of spatial parameters of tidal disruption - There are 3 triangles calculated - for red giants (red, solid line), solar-type stars (blue, dashed line) and white dwarfs (black, dotted line). The interpretation of this diagram follows that only a star within its respective triangle can be tidally disrupted. The upper left corner of the diagram states the conditions for engulfment of small BH by star, while the upper right corner describes the encounter of a star with BH, whose mass is past the Hills mass. The area below the triangles with $\beta < 1$ stands for not fully disruptive tidal encounters. Image credit: Stone [2015].

The Figure 1.2 depicts the scene of tidal disruption, where the star reaches the tidal radius. Soon after that the star will be vertically compressed and partially torn apart. After reaching that point approximately half of the mass will be bound to the SMBH while the other half escapes on a slightly perturbed trajectory. The gas, believed to be major constituent of stars, approaches the SMBH on highly ballistic trajectory accreting onto the SMBH forming the accretion disc, as seen in the Figure 1.2, which appears as luminous transients.

Assuming the Keplerian orbit of stellar debris after the passage of a star around the SMBH the time dependence of the accretion rate of debris is given by $\frac{dM}{dt}$ what can be expressed as $\frac{dM}{d\varepsilon}\frac{d\varepsilon}{dt}$ in which case the parameter ε describes the specific energy of stellar debris, i.e. the energy per unit mass.
The accretion rate can be described by the following formula but only under the assumption that $\frac{dM}{d\varepsilon}$ is at latter stages of accretion flat with the specific orbital energy (Rees [1988])

$$\frac{dM}{dt} = \frac{M_{\rm star}}{3t_{\rm fall}} \left(\frac{t}{t_{\rm fall}} \right)^{-\frac{5}{3}}, \tag{1.5}$$

where $t_{\rm fall}$ is the fall-back timescale of bound debris. The equation 1.5 is applicable only in case that the bolometric luminosity is observed.

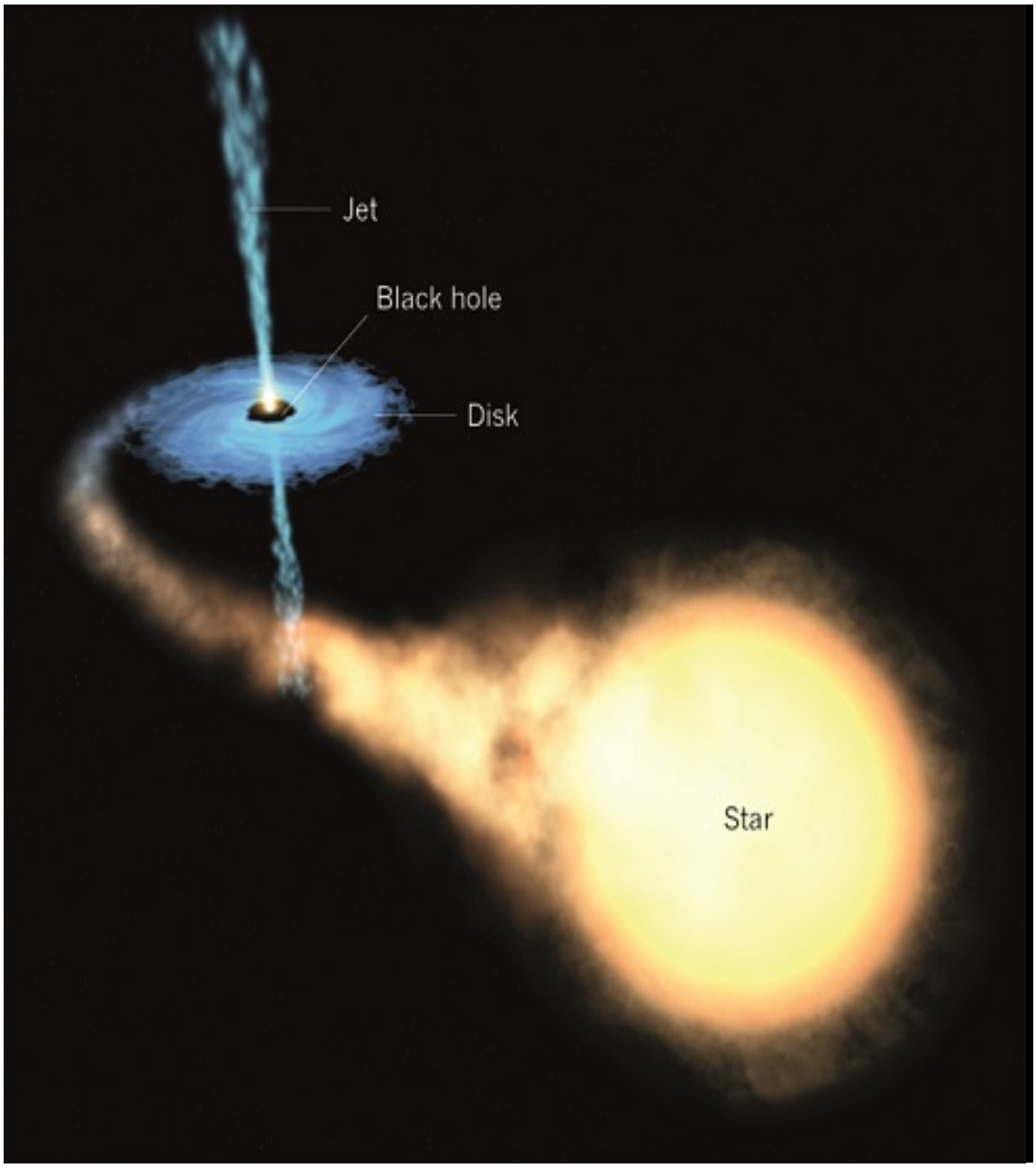

Figure 1.2: Evolution of tidal disruption. Image credit: Umbreit [2012].

1.5 Tidal disruption flares

The difference in the gravitational potential around the SMBH causes the debris to be accreted onto the black hole moving at great speed. This but especially the friction forces raise the temperature of the material invoking the emission of electromagnetic radiation. The electromagnetic radiation spans across all bands with a substantial contribution of X-rays and UV to the observed spectra. The optical radiation is observed too but as a result of reprocessed thermal radiation, which itself is observable at latter stages of the tidal disruption when the density of the nearest circumnuclear material drops.

The observation of spectra emitted during the tidal disruption is what we call a tidal disruption event (TDE hereafter). The characteristic features of a TDE are (see Komossa [2015] if not stated otherwise):

- lightcurves declining at the $t^{-\frac{5}{3}}$, i.e. in agreement with the fall-back model expressed by 1.5,
- soft X-ray spectra that are hardening with years and consistent with the models of TDE accretion discs,
- no activity observed prior to the detection of TDE, i.e. the galaxy and its SMBH was dormant,
- high amplitudes of luminosity in the detected spectra varying in multiple orders in comparison to those observed in active galaxies ,
- bolometric luminosities in the range $10^{45} - 10^{46}$ ergs.s^{-1} peaking in the interval of 0.2 - 2.0 keV (Montesinos Armijo and de Freitas Pacheco [2011]),
- the mass of SMBH residing at the centre of galaxy in interval of 10^6 up to 10^8 masses of sun (see the formula defining the value of Hills mass 1.4).

The TDEs offer a way of proving that there are indeed SMBHs at the centre of each observed galaxy, as proposed by Magorrian et al. [1998]. Most of all they are treated as a valuable tool helping the scientists understand the galactic cores, their history and growth. Such information can be extracted from the value of the BH's spin (see Kerr metric in Kerr [1963]).
Study of BH's spin can be accomplished through the relativistic study of the gravitational shift of the Fe Kα line in the hard X-ray spectra. Zhang et al. [2015] run simulations to infer the BH's spin from the hard X-ray spectra in the case when the TDE flares were observed.

The electromagnetic radiation travelling through the circumnuclear material surrounding the galactic core is being reprocessed due to the interaction with the gas rich environment. The results of studying the spectra behaving in such a way unravels the information regarding its composition. The temporal dependencies found in the X-ray spectra using the reverberation mapping help to determine the size of disruptive and ultimately emitting region of galaxy (e.g. in the case of Swift observation Swift J1644+57 by Kara et al. [2016], etc.). They also enable to

set constraints on the mass of the SMBH at the galactic centre (e.g. in the case of Swift observation Swift J1644+57 by Kara et al. [2016], in case of XMM-Newton observation XMMSL1 J0740-85 by Saxton et al. [2017], etc.).

The formulas characterising the tidal disruption scenario, especially the $t^{-\frac{5}{3}}$-law, also prove to be helpful tools by modelling of the behaviour of black hole binaries (Liu et al. [2014]). Such setting eventually leads to the coalescence of the two BHs, whereas the BH formed as a result of merging can be recoiled in order to conserve the system's momentum.

The jet formation in active galactic nuclei is believed to be the question of magnetohydrodynamical character (Vlahakis and Königl [2004]). According to Spruit and Uzdensky [2005] the magnetic field can be either produced in the disc itself or be advected within the accretion flow. Bloom et al. [2011] were first to apply this to a possible "jetted" TDE candidate Swift J1644+57 asking whether the magnetic field is advected within the accretion flow or if it's generated in the accretion disc considering the magnetohydrodynamical nature of jet. They've come to the conclusion that in the case of Swift J1644+57 the large magnetic field was generated in the disc.

2. Obsevations of TDE

2.1 TDE detection

Detection of TDEs can not be observed by design. Therefore the detectors (X-ray and UV band observations - the Röntgen Satellite (ROSAT), XMM-Newton, Chandra, Suzaku, Swift, the International Gamma-Ray Astrophysics Laboratory (INTEGRAL), the All Sky Automated Survey for Supernovae (ASAS-SN) etc., UV band observations - e.g. the Galaxy Evolution Explorer (GALEX), optical observations - e.g. the Sloan Digital Sky Survey (SDSS)), monitoring the sky usually find the TDEs accidentally (e.g. XMM-Newton during the slew survey).

The crucial part of the observation and precisely the only one that can be planned is the onset of follow-up observations leading to more data. More amount of data leads to the better understanding of the nature of the celestial event, i.e. determining if the approach to the observed celestial event should be pursued or not. In this case if it should be ruled out as a TDE candidate or not. Such an information could be easily gained by the study of the declination of the bolometric luminosity, which in the case involving tidal disruption of a star should obey the $t^{-\frac{5}{3}}$-law.

The TDE rate, i.e. how often such a phenomenon occurs, vary according to the observed spectra. This parameter also depends on the used detectors and their capability of detection. The value of TDE rate based on the observational data is approximately equal to 10^{-5} event/galaxy/year (e.g. Donley et al. [2002]; Gezari et al. [2008]; van Velzen and Farrar [2014]). The estimated number of TDE detected up to date is a little over 60. Table 2.1 shows the TDE candidates estimate along with their name, location and redshift at which it was observed.

The following subsections will provide the status of results drawn from observations of four celestial objects that are considered to be TDE candidates each special in its own way.

Table 2.1: List of TDE candidates (Auchettl et al. [2017])

TDE Name	Host Name	Host R.A. (J2000)	Host Decl. (J2000)	TDE R.A. (J2000)	TDE Decl. (J2000)	Redshift
2MASX J0203	2MASX J02030314-0741514	02:03:03.14	-07:41:51.41			0.0615
2MASX J0249	2MASX J02491731-0412521	02:49:17.32	-04:12:52.20			0.0186
3XMM	3XMM J152130.7+074916	15:21:30.73	+07:49:16.52	15:21:30.75	+07:49:16.70	0.17901
ASASSN-14ze	SDSS J110840.11+340552.2	11:08:40.12	+34:05:52.23	11:08:39.96	+34:05:52.70	0.0436
ASASSN-14li	SDSS J124815.23+174626.4	12:48:15.23	+17:46:26.44	12:48:15.23	+17:46:26.22	0.0206
ASASSN-14oi	2MASX J20390918-3045201	20:39:09.18	-30:45:20.10	20:39:09.10	-30:45:20.71	0.02
ASASSN-14lh	APMUKS(BJ)b215839.70-615403.9	22:02:15.39	-61:39:34.60	22:02:15.45	-61:39:34.64	0.2326
D1-9	GALEX J022517.0-043258	02:25:17.00	-04:32:59.00			0.326
D23H-1	SDSS J233159.53+001714.5	23:31:59.54	+00:17:14.58			01855
D3-13	GALEX J141929.8+525206	14:19:29.81	+52:52:06.37			0.3698
DES14C1kia	Uncatalogued, 03:34:47.49-26:19:35.00	03:34:47.49	-26:19:35.00			0.162
Dougie	SDSS J120847.77+430120.1	12:08:47.78	+43:01:20.27	12:08:47.87	+43:01:20.01	0.191
GRB060218, SN2006aj	SDSS J032139.69+165201.7	03:21:39.69	+16:52:01.74			0.0335
HLX-1	ESO 243-49	01:10:27.75	-49:04:27.41			0.0223
IC 3599	IC 3599	12:37:41.18	+26:42:27.24			0.021245
IGR J12580	NGC 4845	12:58:01.24	+01:34:32.09	12:58:05.09	+01:34:25.70	0.00411
IGR J17361-4441	NGC 6388	17:36:17.46	-44:44:08.34	17:34:17.42	-44:44:05.98	0.04
LEDA 095953	LEDA 095953	13:47:30.10	-32:54:52.00	13:47:30.33	-32:54:50.63	0.0366
NGC 1097	NGC 1097	02:46:19.06	-30:16:29.68			0.0042
NGC 2110	NGC 2110	05:52:11.41	-07:27:22.23			0.007579
NGC 247	NGC 247	00:47:08.55	-20:45:37.44			0.000531
NGC 3599	NGC 3599	11:15:26.95	+18:06:37.33			0.002699
NGC 5905	NGC 5905	15:15:23.32	+55:31:01.59			0.01124
NGC 6021	NGC 6021	15:57:30.68	+15:57:22.37	15:57:30.72	+15:57:21.60	0.015607
PGC 015259	2MPGC 3645	04:29:21.82	-04:45:35.60	04:29:21.84	-04:45:36.00	0.014665
PGC 1127938	2SLAQ J011844.35-010906.8	01:18:44.36	-01:09:06.87	01:18:56.64	-01:03:10.80	0.02
PGC 1185375	2MASX J15035028+0107366	15:03:50.29	+01:07:36.70	15:03:50.40	+01:07:37.20	0.00523
PGC 1190358	N5846-162	15:05:28.75	+01:17:33.17	15:05:28.56	+01:17:31.20	0.00766
PGC 133344	6dFGS gJ214256.0-300758	21:42:55.98	-30:07:57.19	21:52:55.92	-30:07:58.80	0.02365
PGC 170392	6dFGS gJ222646.4-150123	22:26:46.35	-15:01:23.04	22:26:46.32	-15:01:22.80	0.016246
Pictor A	Pictor A	05:19:49.72	-45:46:43.85			0.034
PS1-10jh	SDSS J160928.27+534023.9	16:06:28.28	+53:40:23.99	16:09:28.29	+53:40:23.52	0.1696
PS1-11af	SDSS J095726.82+031400.9	09:57:26.82	+03:14:00.94	09:57:26.82	+03:14:01.00	0.4046
PTF-09axc	SDSS J145313.07+221432.2	14:53:13.08	+22:14:32.27	14:53:13.06	+22:14:32.20	0.1146
PTF-09dil	SDSS J163355.97+301416.6	16:33:55.97	+30:14:16.65	16:33:55.94	+30:14:16.30	0.184
PTF-09ge	SDSS J145703.17+493640.9	14:57:03.18	+49:36:40.97	14:57:03.10	+49:36: 40.80	0.064
PTF-10iam	SDSS J54530.83+540231.9	15:45:30.83	+54:02:31.91	15:45:30.85	+54:02:33.00	0.109
PTF-10iya	SDSS J143840.98+373933.4	14:38:40.98	+37:39:33.45	14:38:41.00	+37:39:33.60	0.22405
PTF-10nuj	SDSS J162624.66+544221.4	16:26:24.66	+54:42:21.44	16:26:24.70	+54:42:21.60	0.132
PTF-11glr	SDSS J165406.16+412015.4	16:54:06.17	+41:20:15.45	16:54:06.13	+41:20:14.80	0.207
RBS 1032	SDSS J114726.69+494257.8	11:47:26.80	+49:42:59.00			0.026
RX J1242-11A	RX J1242.6-1119A	12:42:36.90	-11:19:35.00	12:42:38.55	-11:19:20.80	0.05
RX J1420+53	RX J1420.4+5334	14:20:24.37	+53:34:11.72	14:20:24.20	+53:34:11.00	0.147
RX J1624+75	RX J1624.9+7554	16:24:56.66	+75:54:56.09	16:24:56.70	+75:54:57.50	0.0636
SDSS J0159	SDSS J015957.64+003310.4	01:59:57.64	+00:33:10.49			0.31167
SDSS J0748	SDSS J074820.67+003310.4	07:48:20.67	+47:12:14.23			0.0615
SDSS J0938	SDSS J093801.64+135317.0	09:38:01.64	+13:53:17.08			0.1006
SDSS J0939	SDSS J093922.90+370944.0	09:39:22.89	+37:09:43.90			018589
SDSS J0952	SDSS J095209.56+214313.3	09:52:09.56	+21:43:13.24			0.0789
SDSS J1011	SDSS J101152.98+544206.4	10:11:52.99	+54:42:06.50			0.24608
SDSS J1055	SDSS J105526.41+563713.1	10:55:26.42	+56:37:13.09			0.0743
SDSS J1201	SDSS J120136.02+300305.5	12:01:36.03	+30:03:05.52			0.146
SDSS J1241	SDSS J124134.25+442639.2	12:41:34.36	+44:26:39.23			0.0419
SDSS J1311	SDSS J131122.15-012345.6	13:11:22.15	-01:23:45.61	13:11:22.18	-01:23:45.20	0.18
SDSS J1323	SDSS J132341.97+482701.3	13:23:41.97	+48:27:01.26			0.08754
SDSS J1342	SDSS J134244.41+053056.1	13:42:44.42	+05:30:56.14			0.0366
SDSS J1350	SDSS J135001.49+291609.7	13:50:01.51	+29:16:09.71			0.0777
Swift J1112-82	Swift J1112.2-8238	11:11:47.80	-82:38:47.71	11:11:47.32	-82:38:44.20	0.89
Swift J1644+57	Swift J164449.9+5734.51	16:44:49.30	+57:34:51.00			0.3543
Swift J2058+05	Swfit J205819.7+051329	20:58:19.85	+05:13:33.00			1.1853
UGC 01791	UGC 01791	02:19:53.66	+28:14:52.60	02:19:53.52	+28:14:52.80	0.015881
TDE1,VV-1	SDSS J234201.40+010629.2	23:42:01.41	+01:06:29.30			0.136
TDE2.VV-2	SDSS J232348.61+010810.3	23:23:48.62	-01:08:10.34			0.2515
Wings(A1794)	WINGS J134849.88+263557.5	13:48:49.88	+26:35:57.50	13:48:49.86	+26:35:57.49	0.062
XMMSL1 J0740-85	2MASX J2007400785-8539307	07:40:08.09	-85:39:31.30	07:40:08.43	-85:39:31.4	0.0173

2.2 XMMSL1 J120135.7+300306

On the 10 of June 2010 the XMM-telescope observed during its slew survey sudden activity onset of the galactic core SDSS J120136.02+300305.5 (SDSS J1201+30 hereafter). The event taking place at the centre of the galaxy SDSS J1201+30, moving at the redshift z=0.146, called XMMSL1 J120135.7+300306 was added to the list of TDE candidates (Saxton et al. [2012b]).

The processing of the data by Saxton et al. [2012b] ended up with two reasonable models-first one using the Bremsstrahlung radiation and the second one - Comptonisation model, whereas the Bremsstrahlung radiation model proved to be slightly better fit showing the temperature decline from approximately 390 down to 180 eV corresponding with the drop of X-ray. Saxton et al. [2012a] found out that the radiation taking into account the double power-law also gives a good fit on par with the one assuming the Bremsstrahlung radiation. Possible jet formation as part of XMMSL1 J120135.7+300306 has been ruled out based on the radio observations (Saxton et al. [2012b]).

Further results drawn by the study of observational data provided thanks to follow-up programs by Swift and XMM-Newton telescopes confirmed the luminosity decline following $t^{-\frac{5}{3}}$-law. The calculations carried out by Liu et al. [2009] describe the tidal disruption scenario occurring in the presence of two SMBHs, i.e. super-massive black hole binaries (SMBHB hereafter). The lightcurve depicting luminosity's dependence on time showed vacancies at a couple of places, which means the detectors didn't receive any radiation. Liu et al. [2014] showed that the lighcurves and their vacant places of XMMSL1 J120135.7+300306 are in agreement with the tidal disruption scenario located in the system with two SMBHs, where one of them is tidally disrupting the star while the other one acts as a perturber.

2.3 Gas cloud in Milky-Way

In 2011 scientists discovered at first an unidentified object approaching the periapsis (in this case peribothron) of the SMBH Sagittarius A* that is supposed to reside at core of the Milky-Way galaxy (see Genzel et al. [2000] and references therein). The object assigned the name G2 was believed to be a gas cloud that was about to reach the critical point in the year 2013 with an innermost approach of approximately 3100 times the event horizon (Gillessen et al. [2012]).

Gas clouds are suspected to be behind the outbursts of radiation received from the source Sagittarius A* according to Clavel et al. [2013] and Czerny et al. [2013]. G2 was spotted before actually reaching the point of tidal disruption. This could have enabled the scientists to observe planned TDE and to probe the properties of the accretion flow and the feeding processes involving the SMBH at the centre of our galaxy (Gillessen et al. [2012]).

Since the G2 remained compact after its passage around the SMBH at centre of our galaxy a question has arisen regarding the nature of the observed object. According to Miralda-Escudé [2012] the celestial object G2 is not a gas cloud, as anticipated but an old low-mass main-sequence star with a gas disc around it. The reason why the observed object was being perceived as a gas cloud, i.e. engulfed by the gas envelope, could be caused by the ejection of gas caused by the shocks induced by passing around the compact objects. Such an object could have been formed during the previous interaction of the star with the compact objects (e.g. a SMBH) interrupting the process of tidal disruption.

The explanation proposed by Miralda-Escudé [2012] would make much more sense in relation to the results of the observation and to the fact that self-gravity of a gas cloud could not withstand the gravitational pull of SMBH. Zajaček et al. [2014] back up the theory regarding tidal disruption of gas cloud approaching the SMBH and take also into account the possibility that there's a star wrapped up in the gas envelope. Moreover they bring forward an interesting alternative that there could be a binary star embedded in the gas envelope. They state that the second peribothron passage of G2 could shed some light on the nature of the celestial object.

2.4 GRB 110328A/Swift J164449.3+573451

The Swift Burst Alert telescope detected on the 28-th of March 2011 the high-energy burst coming from the centre of the compact, star-forming and otherwise quiescent galaxy (Burrows et al. [2011]) with redshift z=0.3534 (Levan et al. [2011]). This celestial event first assigned the name GRB 110328A was considered to be a gamma ray burst (Cummings et al. [2011]). In terms of definition of gamma ray bursts the high-energetic bursts should be observed only for a short period of time. The GRB 110328A's radiation not only had longer duration than expected but they did not even fade in a way the gamma ray bursts would. That, having a peak luminosity up to 10^{48} erg.s^{-1} and bolometric luminosity decay following the $t^{-\frac{5}{3}}$-law led to the change of the opinion of science community and the celestial event started to be treated as a TDE involving the jet formation being referred to as Swift J164449.3+573451 (Swift J1644+57 hereafter).

Right now Swift J1644+57 is considered to have the best covered lightcurve among all the TDEs so far with a sudden drop of X-ray radiation at approximately 500 day causing it undetectable for Swift detectors (Komossa [2015]). The radiation from radio band was on the other hand not showing any signs of decline implying that the X-ray and radio source don't have the same place of origin (Komossa [2015]).
There is also a mysterious re-brightening in the radio-band 6 months after that lasted for about 1 month. According to Metzger et al. [2012] the observed effect could be caused by the complex jet structure, which can be only verified by another similar observation or successful simulation.

The follow-up observations set on after the initial discovery enabled studying the timelags of the spectra using the reverberation techniques leading to the

constraining of the central emitting region to tens of gravitational radii and approximate estimation of the mass of the galactic core (Kara et al. [2016]).
According to Kara et al. [2016] and Metzger et al. [2012] the jet is suspected to be narrowly collimated, which is according to the results of the study involving the iron Fe Kα line (Kara et al. [2016]), observable in this case, caused by the presence of funnel wall made of outflowing material accelerated to the speeds 0.1c-0.5c. An interesting case of tidal disruption scenario, precisely TDE involving jet formation, is Swift J2058.4+0516 (Swift J2058+05 hereafter) first reported by Cenko et al. [2012]. According to Cenko et al. [2012] Swift J2058+05 launched an extremely narrow jet. The similarity of both of these celestial objects (Swift J1644+57 and Swift J2058+05) called into question the conditions under which the jet formation can take place, i.e. requirements for the generation of a large-scale magnetic field, type of tidally stripped star and its trajectory, etc.

2.5 XMMSL1 J074008.2-853927

One of the traits of TDEs is that they posses either a hard X-ray component or a thermal one. The question why the components should be separated, if they even are separated, is still open (e.g. Komossa [2002]). XMMSL1 J074008.2-853927 (XMMSL1 J0740-85 hereafter) observed on the 1-st of the April 2014 by XMM-Newton telescope is a TDE candidate possessing both thermal and non-thermal radiation components. Furthermore this TDE is suspected to show signs of an iron line emission in the X-ray spectra.

The hard and soft X-ray components declined, as predicted, following the fall-back rate $t^{-\frac{5}{3}}$-law, while the decrement of UV radiation, supposedly thermal component, was not as steep as X-ray's and was best fit by $t^{-1.2}$ (Saxton et al. [2017]).
The data from the first XMM-Newton follow-up observation (30-th of April 2014) fit by Saxton et al. [2017] gave the best fit by using power-law model combined with either black-body model component or Bremsstrahlung radiation component. The best-fit candidates for the spectral data from the second XMM-Newton follow-up observation (12-th of January 2015) involve double power-law model and power-law model with Bremsstrahlung radiation component.

The reverberation techniques used by Saxton et al. [2017] set the conditions on the size of the emitting region leading to the estimated value of 400 lightseconds or equivalently 1.2×10^{13} cm, while the X-ray variability constrained the BH's mass to $1 \times 10^6 M_\odot < M_{\mathrm{BH}} < 1 \times 10^7 M_\odot$. They also determined that the energy released up to the 285-th day from the post-starburst discovery XMMSL1 J0740-85 accounting for 5×10^{50} erg.s^{-1} corresponds to the 0.025 $M_\odot$ of consumed mass of the star.

The prediction based on the past observations stating that the soft X-ray hardens with time (e.g. Komossa and Bade [1999]) held true. The observations in the radio band indicated the same position of the source as the ones done by Swift and XMM telescopes (Saxton et al. [2017]). Even though the radio emission has the same site of origin as XMMSL1 J0750-85 it is debatable if they are entangled. An

interesting theory proposed by Saxton et al. [2017] resolving the problem with the radio emission is based on comparison XMMSL1 J0750-85 with NGC 4845, which could be according to radio emission (Irwin et al. [2015]) a product of an off-axis relativistic jet (Lei et al. [2016]). On the other hand Alexander et al. [2016] state that the XMMSL1 J0750-85's outflow is non-relativistic bearing resemblance to the TDE ASASSN-14li.

3. Spectral re-analysis of XMMSL1 J0740-85

Prior to the tidal disruption XMMSL1 J0740-85 was found to be a non-active galaxy at a redshift z=0.0173 (Saxton et al. [2017]) (see Section 2.5).
The additional study of optical spectra conducted by Saxton et al. [2017], based on observational data by 2MASS redshift survey and the WFCCD imagerspectrograph, showed that the emission is represented by the 2 Gyr old young stellar population, whereas the old stellar population stands behind the majority of mass in the galaxy. This makes the XMMSL1 J0740-85 a part of a larger group of TDEs that took place in post-starburst galaxies - a common feature first noticed by Arcavi et al. [2012].

In the following section we present the results of spectral re-analysis of X-ray observation of XMMSL1 J0740-85. We employed the models by Saxton et al. [2017] and extended this analysis by detailed study of residuals in the iron line band and the soft excess.

3.1 Observations

The XMM-Newton telescope undertook the first follow-up observation 29 days after the initial discovery of XMMSL1 0740-85.29. This first follow-up observation was performed on the 30-th April 2014 and the second observation on the 12-th of January 2015. Both observations were performed using the European Photon Imaging Cameras (EPIC) - PN and MOS-1 that were operating in the full frame mode.

We used the same data as reduced by Saxton et al. [2017] with Science Analysis System (SAS) version $20141104\_1833 - 14.0.0$. The exposure time accounted for 26.6 ks (in case of the first XMM-Newton follow-up observation) and 16.1 ks (in case of the second XMM-Newton follow-up observation).

For fitting the X-ray spectra we used the Xspec software package version 12.9.0. All the spectral fits were performed in the interval of 0.3 - 10.0 keV if not stated otherwise, whereas we used the chi-square statistical test (χ^2 statistic hereafter) to judge the quality of given models[1]. The spectra were grouped so that the minimal amount of counts per bin is equal to 25 (in case of the first XMM-Newton follow-up observation) and to 20 (in case of the second XMM-Newton follow-up observation) to satisfy the usage of χ^2 statistic.

[1]The quality of a model can be judged by reduced chi-squared statistic, where the value of reduced chi-squared (χ^2_r) for a given model, defined as quotient of chi-squared (χ^2) and degrees of freedom (d.o.f. hereafter), should be ideally near the value of 1.

3.2 Models

The model components we used in all models included the simple power-law component `powerlaw` accompanied by the Galactic column density component `TBABS` (Wilms et al. [2000]). Afterwards we started adding model components - black-body component `bbody`, thermal component modelling the temperature profile of radiation, reflection component `reflionx` (Ross and Fabian [2005]) convolved with `kdblur` (Fabian et al. [2002]) component or Bremsstrahlung component `brems`. In two models we also used multiplicative model component `zxicpf` that stands for ionized absorber (Reeves et al. [2008]).
Further we added `laor` component (Laor [1991]) to the best-fit models for both XMM-Newton follow-up observations. In case of the first XMM-Newton follow-up observation we also added to the best-fit models the `zgauss`.

We set the abundance table option to wilm, whereas the abundances are set to zero value except for the elements that are not included in the paper by Wilms et al. [2000]. To model the absorption due to its passage through the Galactic column we used the `TBABS` model component, where the only variable element component is Hydrogen. The numerical value of the Galactic column density was $N_H = 1.5 \times 10^{21}$ cm^{-2} (Saxton et al. [2017]).

The fact that we had at disposal two data sets for each observation necessitated the presence of cross-calibration constant in each model. We run fitting procedure for each model so that we kept the cross-calibration constant fixed to 1 for PN data, whereas the cross-calibration constant for MOS-1 data was a free parameter. The differences in the cross-calibration constants in each model for both data sets should ideally not exceed 10 % (Read et al. [2014]).

The power-law component, measuring the dependence of radiative flux density on frequency, is characterised by the slope index Γ as well as the normalisation factor.
The black-body component, thermal component describing the temperature profile, is characterised by the temperature of radiation and its normalisation factor. Similarly the Bremsstrahlung component, modelling the circular motion of hot charged particles, i.e. plasma, is represented by set of two parameter the temperature of hot plasma and its normalisation factor. The black-body component could point out to the existence of accretion disc around the BH, whereas the Bremsstrahlung component is usually associated with jet formation.
The reflection component has five parameters. The ionisation parameter ξ, the normalisation factor of the reflected spectrum, the ratio of abundance of iron to solar value, the power-law index and redshift z. The convolution model `kdblur` is represented by four parameters: the emissivity index, the inner radius of accretion disc $R_{\mathrm{in\_G}}$, the outer radius of accretion disc $R_{\mathrm{out\_G}}$ and the inclination of the radiation source. The reflection component is used to model the reprocessed emission, which originates by the irradiation of an optically thick medium by the hard X-ray flux, whereas the convolution model component `kdblur` covers the effects of general relativity in the vicinity of the BH.
The significant parameters of ionised absorber model component, used to model

the additional partially ionized material that reprocesses the emitted radiation, are the column density of partially ionised material $N_{\rm H}$, the logarithm of ionisation factor ξ and the covering factor $c_{\rm f}$.

The `zgauss` component, computing the redshifted gaussian function, is described by the line energy $E_{\rm line}$, the line width σ and its normalisation constant. The `laor` component is characterised by the line energy $E_{\rm line}$, the emissivity index, the inner radius of accretion disc $R_{\rm in\_G}$, the outer radius of accretion disc $R_{\rm out\_G}$, redshift z, the inclination of the radiation source and the normalisation factor. It is used to model the relativistic effects on the emission line coming from the accretion disc around the BH.

The syntax describing the structure of each model is reported in Table 3.1.

Table 3.1: Models used to fit data from XMM follow-up observations

	Model Component
Models	(Power-law + Power-law)
	(Power-law + Black-body)
	(Power-law + Bremsstrahlung)
	(Power-law + kdblur $\bigotimes$ Reflection[a])
	(Power-law × Ionized absorber)
	(Power-law + Black-body) × Ionized absorber

[a] $\bigotimes$ symbolises the convolution
All the model were multiplied by the cross-calibration constant and `TBABS` component for Galactic column absorption.

3.3 Results

3.3.1 The first observation

The first XMM-Newton follow-up observation (XMM1 observation hereafter) of XMMSL1 J0740-85 was performed on the 30-th of April 2014. When analysing the spectra for XMM1 observation we approached the data analysis the same way as Saxton et al. [2017] and used all the models proposed by them.

Fitting the data with the simple power-law model including the absorption by the Galactic column density, $N_H = 1.5 \times 10^{21}$ cm^{-2} lead to $\Gamma = 3.80 \pm 0.04$, Norm $= 2.15 \pm 0.04 \times 10^{-4}$ keV^{-1}cm^{-2}s^{-1} and χ^2 of 1774 for 399 d.o.f. Therefore we started altering the model by adding extra components to improve the fit statistics. The extra power-law component added to the model gave the slope index $\Gamma = 4.61 \pm 0.08$ for the first power-law and $\Gamma = 1.43 \pm 0.09$ for the second one with χ^2 of 516 for 397 d.o.f. The black-body component gave a fit with the power-law slope $\Gamma = 1.94 \pm 0.06$, the temperature kT $= 86 \pm 2$ eV and χ^2 of 415 for 397 d.o.f. With the Bremsstrahlung component the fit gave the power-law slope index $\Gamma = 1.82 \pm 0.06$, the plasma temperature kT $= 170 \pm 5$ eV and χ^2 of 414 for 392 d.o.f. The reflection component convolved with `kdblur` lead to the power-law slope index $\Gamma = 1.23 \pm 0.09$, the ionisation factor $\xi = 650^{+360}_{-120}$ erg$\frac{\text{cm}}{\text{s}}$ and χ^2 of 589 for 395 d.o.f. During the fitting procedure testing this model we set the emissivity index to 3, the inner radius of accretion disc $R_{\text{in\_G}}$ to 4.5 R_g, the outer radius of accretion disc $R_{\text{out\_G}}$ to 100 R_g and the inclination of radiation source to 45°, as used by Saxton et al. [2017]. After the usage of ionised absorber component we obtained the power-law slope index $\Gamma = 3.34 \pm 0.04$, the ionised material's column density $N_H = 17.5^{+0.9}_{-1.0}$ cm^{-2} and χ^2 of 460 for 396 d.o.f. The combination of black-body component with ionised absorber component gave the power-law slope index $\Gamma = 2.45^{+0.21}_{-0.20}$, the temperature kT $= 86^{+4}_{-3}$ eV, the ionised material's column density $N_H = 18.0^{+4.2}_{-2.9}$ cm^{-2} and χ^2 of 383 for 394 d.o.f. The results of fitting procedure of XMM1 data along with the quality of given model are reported in Table 3.2.

The best-fit candidates are the ones with extra black-body and Bremsstrahlung component. Neither the double power-law model, the power-law with intrinsic absorber, nor the power-law with black-body and intrinsic absorber gave a good fit. The extra black-body component together with intrinsic absorber gave χ^2_r smaller than 1. The result of F-test with the probability of 2.12×10^{-16} revealed that adding black-body component to the model involving intrinsic absorber was statistically significant. The Figure 3.1 shows the observed spectra, best-fit model with extra Bremsstrahlung component and the data residuals. The Figure 3.2 shows the observed spectra, the model with extra black-body and ionised absorber component and the data residuals.

Table 3.2: Spectral fits for XMM1 observation

Power-law		second Power-law		Black-body		Bremsstrahlung		Reflection		Ionised absorber			χ^2_r
Γ	Norm	Γ	Norm	kT	Norm	kT	Norm	ξ	Norm	N_H	log(ξ)	c_f	
	$keV^{-1}cm^{-2}s^{-1}$		$keV^{-1}cm^{-2}s^{-1}$	eV	[2]	eV	[3]	$erg\frac{cm}{s}$	$\times 10^{-8}$	$10^{22}cm^{-2}$		%	
4.61 ± 0.08	$1.26 \pm 0.08 \times 10^{-4}$	1.43 ± 0.09	$5.42^{+0.65}_{-0.62} \times 10^{-5}$										$\frac{516}{397}$
1.94 ± 0.06	$1.13^{+0.06}_{-0.05} \times 10^{-4}$			86 ± 2	$2.80^{+0.13}_{-0.12} \times 10^{-5}$								$\frac{415}{397}$
1.82 ± 0.06	$9.81^{+0.60}_{-0.59} \times 10^{-5}$					170 ± 5	$1.01^{+0.09}_{-0.08} \times 10^{-2}$						$\frac{414}{397}$
1.29 ± 0.09	$4.44^{+0.54}_{-0.50} \times 10^{-5}$							650^{+360}_{-120}	$2.9^{+1.2}_{-1.1}$				$\frac{589}{395}$
3.31 ± 0.04	$1.72^{+0.21}_{-0.20} \times 10^{-3}$									$17.5^{+0.9}_{-1.0}$	$1.95^{+0.02}_{-0.01}$	92 ± 1	$\frac{460}{396}$
$2.45^{+0.21}_{-0.20}$	$4.0^{+1.9}_{-1.3} \times 10^{-4}$			86^{+4}_{-3}	$5.9^{+1.4}_{-1.2} \times 10^{-5}$					$18.0^{+4.2}_{-2.9}$	$1.96^{+0.08}_{-0.38}$	68^{+9}_{-13}	$\frac{383}{394}$

All listed errors are 90 % confident.

[2] $\frac{L}{D}$, where L is the luminosity of the source in $10^{39}\frac{erg}{s}$ and D is the distance to the source in 10 kpc

[3] $\frac{3.02\times10^{-15}}{4\pi D^2} \int n_e n_i dV$, where D is the distance to the source in cm, n_e and n_i are electron and ion densities in cm^{-3}

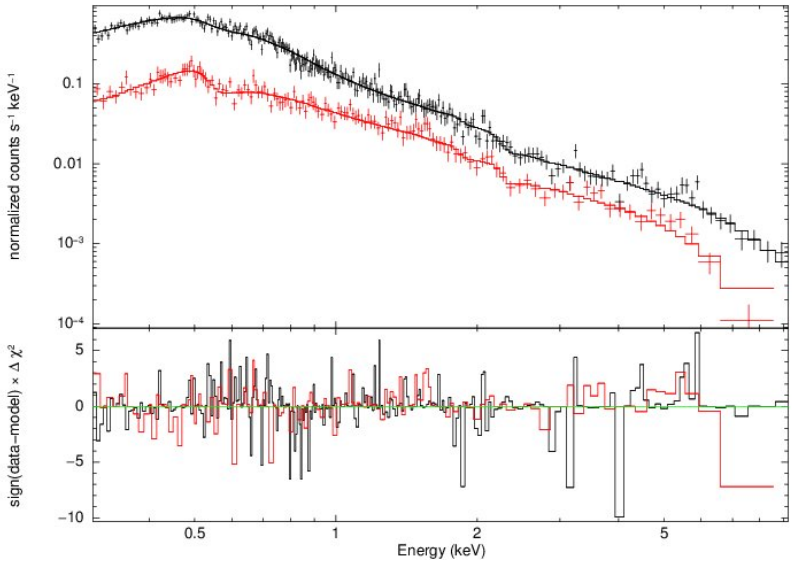

Figure 3.1: Up: PN (black line) and MOS-1 (red line) spectra from XMM1. Bottom: Data residuals from the model fit, power-law model with extra Bremsstrahlung component.

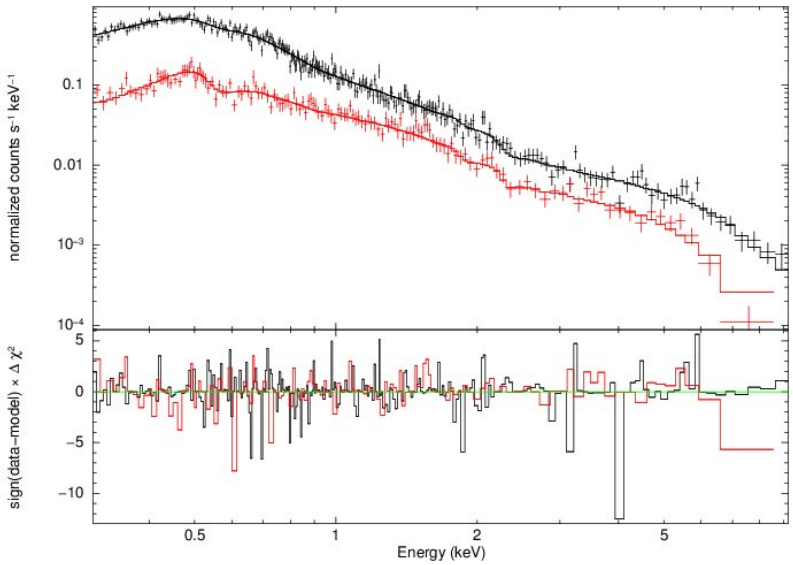

Figure 3.2: Up: PN (black line) and MOS-1 (red line) spectra from XMM1. Bottom: Data residuals from the model fit, power-law model with extra black-body and ionised absorber component.

3.3.2 The second observation

The second XMM-Newton follow-up observation (XMM2 observation hereafter) of XMMSL1 J0740-85 was performed on the 12-th of January 2015. The models we implemented in case of the spectral analysis of XMM2 observation were proposed by Saxton et al. [2017].

Following the same procedure as we did when analysing the spectra of XMM1 observation we tried the simple power-law model including the Galactic column density $N_H = 1.5 \times 10^{21}$ cm^{-2}. We obtained the value of the slope index $\Gamma = 3.08^{+0.07}_{-0.06}$, Norm $= 1.57 \pm 0.05 \times 10^{-4}$ keV^{-1}cm^{-2}s^{-1} and χ^2 of 247 for 107 d.o.f. The extra power-law component added to the model gave the slope index $\Gamma = 4.14^{+0.41}_{-0.32}$ for the first power-law, $\Gamma = 1.94^{+0.24}_{-0.29}$ for the second one and the χ^2 of 115 for 105 d.o.f. The black-body component gave a fit with the power-law slope $\Gamma = 2.38 \pm 0.11$, the temperature kT $= 85 \pm 7$ eV and χ^2 of 102 for 105 d.o.f. The result of adding extra Bremsstrahlung component lead to the fit with the power-law slope index $\Gamma = 2.29 \pm 0.13$, the plasma temperature kT $= 180^{+24}_{-23}$ eV and χ^2 of 116 for 105 d.o.f. After the entering the ionised absorber component we obtained the power-law slope index $\Gamma = 3.07^{+0.27}_{-0.07}$, the ionised material's column density 14^{+3}_{-9} and χ^2 of 122 for 104 d.o.f. The black-body component together with ionised absorber component gave the power-law slope index $\Gamma = 2.80 \pm 0.39$, the temperature kT $= 76^{+9}_{-15}$, the ionised material's column density $N_H = 6^{+94}_{-3}$ and χ^2 of 116 for 102 d.o.f. The results of fitting procedure of XMM2 data along with the quality of given model are reported in Table 3.3.

The best-fit candidates for this observation are the models with extra power-law and Bremsstrahlung component. For the remaining models - neither the extra black body component, the ionized absorber component, nor their combination lead to a good fit. The Figures 3.3 and 3.4 show the observed spectra of XMM2, the implemented best-fit model and data residual for given fit respectively. Similarly as for the XMM1 observation there is almost no difference in the data residuals (see Figure 3.1 and 3.2). It is due to the fact that both models for both XMM-Newton follow-up observations fit the data equally good across the noticed energies.

Table 3.3: Spectral fits for XMM2 observation

Power-law		second Power-law		Black-body		Bremsstrahlung		Ionised absorber			χ^2_r
Γ	Norm	Γ	Norm	kT	Norm	kT	Norm	N_H	$\log(\xi)$	c_f	
	$keV^{-1}cm^{-2}s^{-1}$		$keV^{-1}cm^{-2}s^{-1}$	eV		eV		$10^{22}cm^{-2}$		%	
$4.14^{+0.41}_{-0.32}$	$7.3^{+2.5}_{-2.4} \times 10^{-5}$	$1.94^{+0.24}_{-0.29}$	$6.3^{+2.3}_{-2.2} \times 10^{-5}$								$\frac{115}{105}$
2.38 ± 0.11	$(1.15 \pm 0.09) \times 10^{-4}$			85 ± 7	$9.2^{+1.7}_{-1.3} \times 10^{-6}$						$\frac{122}{105}$
2.29 ± 0.13	$(1.05 \pm 0.12) \times 10^{-4}$					180^{+24}_{-23}	$3.13^{+1.19}_{-0.75} \times 10^{-3}$				$\frac{116}{105}$
$3.07^{+0.27}_{-0.07}$	$5.2^{+2.2}_{-1.5} \times 10^{-4}$							14^{+3}_{-9}	$1.8^{+0.8}_{-1.4}$	74^{+7}_{-11}	$\frac{122}{104}$
2.80 ± 0.39	$3.4^{+3.4}_{-2.0} \times 10^{-4}$			76^{+9}_{-15}	$2.1^{+2.6}_{-1.1} \times 10^{-5}$			6^{+94}_{-3}	$-0.55^{+2.37}_{+0.55}$	62^{+19}_{-39}	$\frac{116}{102}$

All listed errors are 90 % confident.

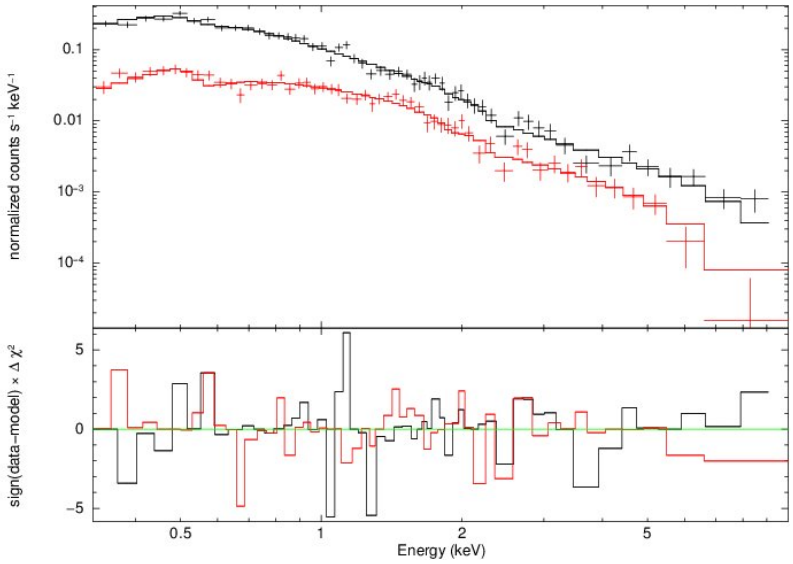

Figure 3.3: Up: PN (black line) and MOS-1 (red line) spectra from XMM2. Bottom: Data residuals from the model fit, power-law model with extra power-law component.

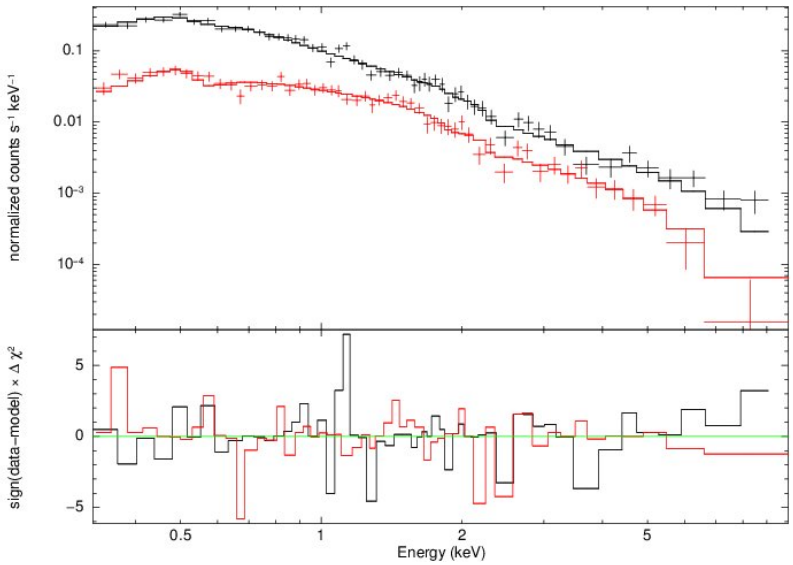

Figure 3.4: Up: PN (black line) and MOS-1 (red line) spectra from XMM2. Bottom: Data residuals from the model fit, power-law model with extra Bremsstrahlung component.

3.4 Detailed look at the Fe Kα line band residuals and the soft energy excess

Saxton et al. [2017] noticed that there is an energy excess around 6 keV in the spectra of XMM1 observation. They proposed that it could be caused by the presence of Fe Kα line and tried to model it using the model `TBABs*optxagnf*zxipcf`. We attempted to approach the problem similarly. However, to model the energy excess we added `laor` component to all best-fit models for XMM1 and subsequently XMM2 observation. The fitting procedure was done in interval of 1 - 10 keV.

First we tried to model the iron line emission by adding the `zgauss` component to both best-fit models. We obtained $\mathrm{E_{line}} = 5.63^{+0.17}_{-0.50}$ keV and $\sigma = 0.30^{+0.64}_{-0.21}$ keV (model with extra black-body component) and $\mathrm{E_{line}} = 5.63^{+0.17}_{-0.50}$ keV and $\sigma = 0.30^{+0.63}_{-0.21}$ keV (model with extra Bremsstrahlung component).
The results of the application of `laor` component to the XMM1 observation lead, in case of extra black-body component, to the emission line $\mathrm{E_{line}} = 5.33^{+0.13}_{-0.24}$ keV and χ^2 of 163 for 188 d.o.f. For the model involving extra Bremsstrahlung component we obtained the emission energy line $\mathrm{E_{line}} = 5.34^{+0.12}_{-0.24}$ keV and χ^2 of 163 for 188 d.o.f. We got both of these results when setting the emissivity index to 3, the inner radius of accretion disc $R_{\mathrm{in\_G}}$ to 4.5 $\mathrm{R_g}$, the outer radius of accretion disc $R_{\mathrm{out\_G}}$ to 100 $\mathrm{R_g}$ and the inclination of radiation source to 45°, similarly as the conditions proposed by Saxton et al. [2017] when using `kdblur` component. The second time we ran the fitting procedures while keeping the value of outer radius of accretion disc $R_{\mathrm{out\_G}}$ fixed to 100 $\mathrm{R_g}$. We obtained $\mathrm{E_{line}} = 4.94^{+0.10}_{-0.47}$ keV and χ^2 of 161 for 186 d.o.f. for the model with extra black-body component and $\mathrm{E_{line}} = 5.01^{+0.39}_{-0.44}$ keV and χ^2 of 161 for 186 d.o.f. for the model with extra Bremsstrahlung component. We obtained the emission line $\mathrm{E_{line}} = 6.87^{+0.24}_{-0.23}$ keV and χ^2 of 160 for 185 d.o.f. for extra black-body component and $\mathrm{E_{line}} = 6.12^{+0.16}_{-0.37}$ keV and χ^2 of 160 for 185 d.o.f. for extra Bremsstrahlung component when letting all parameters of `laor` component be free, except for the emissivity index that was set to 3.

After the application of `laor` component to the XMM2 observation best-fit models we obtained $\mathrm{E_{line}} = 3.22^{+0.10}_{-0.09}$ keV and χ^2 of 68 for 61 d.o.f. for extra power-law component and $\mathrm{E_{line}} = 3.00^{+0.07}_{-0.05}$ keV and χ^2 of 67 for 61 d.o.f. for extra Bremsstrahlung component. Fitting was performed allowing all parameter to be free, except for the emissivity index that was set to 3.

The results of fitting procedure of the best-fit models for XMM1 and XMM2 observation after adding `laor` component are reported in Table 3.4 along with the quality of given model.

We calculated the equivalent width of the iron line emission for both XMM1 and XMM2 observations when adding `laor` component to the best-fit models, keeping all parameters free. In case of XMM1 observation we obtained the equivalent width of $0.90^{+0.42}_{-0.35}$ keV for extra black-body component and 0.88 ± 0.35 keV for extra Bremsstrahlung component, whereas in case of XMM2 observation we obtained the equivalent width of $0.22^{+0.14}_{-0.13}$ keV for extra power-law component

and $0.26^{+0.13}_{-0.15}$ keV for extra Bremsstrahlung component. The F-test unfolded that adding `laor` component, keeping values proposed by Saxton et al. [2017], to the best-fit models for XMM1 observations was statistically significant with probability of 11×10^{-3} for both extra black-body component and extra Bremsstrahlung component. The F-test results are the same when taking into account the possibility of free parameters. However, the F-test in case of XMM2 observation revealed that adding `laor` component, with all parameters free, was not statistically significant with probability of 0.55 for extra power-law component and 0.47 for extra Bremsstrahlung component.

We checked the dependence of χ^2 on parameters of `laor` component that even if being all free give almost the same fit goodness as fixed parameter chosen by Saxton et al. [2017], i.e. $\Delta\chi^2 = 2$ for 2 d.o.f. in case of fixed value of the outer radius of accretion disc $R_{\mathrm{out\_G}}$ to 100 $\mathrm{R_g}$ and $\Delta\chi^2 = 3$ for 3 d.o.f. for all parameters being free (see Table 3.4). Given the fact that the fit goodness of both best-fit models after adding `laor` component do not differ, i.e. are consistent with each other, we proceeded with the best-fit model involving extra Bremsstrahlung component. The Figure 3.5 shows that inner radius of accretion disc $R_{\mathrm{in\_G}}$ can not be constrained. Similar is the situation depicted in the Figure 3.6 showing that almost all values of the outer radius of accretion disc $R_{\mathrm{out\_G}}$ belong to the 90 % confidence region. The Figure 3.7 shows the same for the inclination of the radiation source, whose all values bigger than approximately 25° belong to the 90 % confidence region. The F-test probability of 0.33 also points out that letting all parameters be free is not statistically significant.

The results for XMM1 observation indicate that there is indeed a possible presence of Fe Kα line emission or ionised Fe Kα line emission. The spectrum of XMM2 observation shows no energy excess at such energies in comparison to those observed and well fit in the spectrum of XMM1 observation (see Figure 3.8). The Fe Kα line is either not present or it could be moved to the lower energies, as the material approached the SMBH.

Table 3.4: Spectral fits for XMM1 and XMM2 observation involving line emission

XMM1 observation											
Power-law		Black-body		Bremsstrahlung		`laor`					χ^2_r
Γ	Norm	kT	Norm	kT	Norm	E_{line}	R_{in_G}	R_{out_G}	Inclination	Norm	
	$keV^{-1}cm^{-2}s^{-1}$	eV		eV		keV	R_g	R_g	$\circ$	$cm^{-2}s^{-1}$	
$1.89^{+0.12}_{-0.13}$	$9.8^{+1.3}_{-1.4} \times 10^{-5}$	140 ± 43	$3.4^{+1.4}_{-1.7} \times 10^{-6}$			$5.33^{+0.13}_{-0.24}$	fixed to 4.5	fixed to 100	fixed to 45	$(3.1 \pm 1.3) \times 10^{-6}$	$\frac{163}{188}$
$1.88^{+0.13}_{-0.15}$	$9.6^{+1.4}_{-1.6} \times 10^{-5}$			250^{+140}_{-100}	$1.7^{+23.9}_{-1.3} \times 10^{-3}$	$5.34^{+0.12}_{-0.24}$	fixed to 4.5	fixed to 100	fixed to 45	$(3.09 \pm 1.3) \times 10^{-6}$	$\frac{163}{188}$
1.92 ± 0.13	$1.00^{+0.13}_{-0.20} \times 10^{-4}$	140^{+44}_{-45}	$3.6^{+21.5}_{-2.1} \times 10^{-6}$			$4.95^{+0.10}_{-0.47}$	$9.6^{+32.6}_{-9.6}$	fixed to 100	66^{+20}_{-40}	$3.6^{+1.6}_{-2.4} \times 10^{-6}$	$\frac{161}{186}$
$1.91^{+0.13}_{-0.15}$	$1.0^{+1.3}_{-1.5} \times 10^{-5}$			230^{+152}_{-96}	$2.3^{+8.9}_{-1.8} \times 10^{-3}$	$5.01^{+0.39}_{-0.44}$	$8.3^{+36.1}_{-8.3}$	fixed to 100	60^{+27}_{-42}	$3.5^{+1.6}_{-1.3} \times 10^{-6}$	$\frac{161}{186}$
$1.91^{+0.12}_{-0.13}$	$1.0^{+1.3}_{-1.4} \times 10^{-5}$	140 ± 43	$3.6^{+12.1}_{-2.0} \times 10^{-6}$			$6.87^{+0.24}_{-0.23}$	$5.21^{+0.36}_{-1.55}$	$5.69^{+2.11}_{-0.80}$	19^{+3}_{-6}	$(3.2 \pm 1.3) \times 10^{-6}$	$\frac{160}{185}$
1.89 ± 0.09	$9.8^{+1.2}_{-1.6} \times 10^{-5}$			240^{+110}_{-99}	$2.0^{+3.9}_{-1.5} \times 10^{-3}$	$6.12^{+0.16}_{-0.61}$	$8.0^{+1.8}_{-3.4}$	$8.6^{+8.1}_{-2.6}$	24^{+3}_{-5}	$(3.1 \pm 1.2) \times 10^{-6}$	$\frac{160}{185}$
XMM2 observation											
Power-law		second Power-law		Bremsstrahlung		`laor`					χ^2_r
Γ	Norm	Γ	Norm	kT	Norm	E_{line}	R_{in_G}	R_{out_G}	Inclination	Norm	
	$keV^{-1}cm^{-2}s^{-1}$		$keV^{-1}cm^{-2}s^{-1}$	eV		keV	R_g	R_g	$\circ$	$cm^{-2}s^{-1}$	
$-0.05^{+4.52}_{-2.37}$	$7.3^{+823.4}_{-7.7} \times 10^{-7}$	$2.62^{+0.35}_{-0.23}$	$(1.21 \pm 0.11) \times 10^{-4}$			$3.22^{+0.10}_{-0.09}$	$19.56^{+0.12}_{-2.29}$	$20.17^{+0.68}_{-0.19}$	24^{+5}_{-7}	$2.1^{+1.3}_{-1.2} \times 10^{-6}$	$\frac{68}{61}$
$1.42^{+0.72}_{-1.01}$	$2.6^{+5.6}_{-2.2} \times 10^{-5}$			830^{+390}_{-380}	$2.15^{+0.89}_{-0.92} \times 10^{-4}$	3.06 ± 0.08	$31.10^{+0.65}_{-3.37}$	$32.98^{+2.36}_{-0.29}$	25^{+7}_{-13}	$(2.4 \pm 1.3) \times 10^{-6}$	$\frac{67}{61}$

All listed errors are 90 % confident.

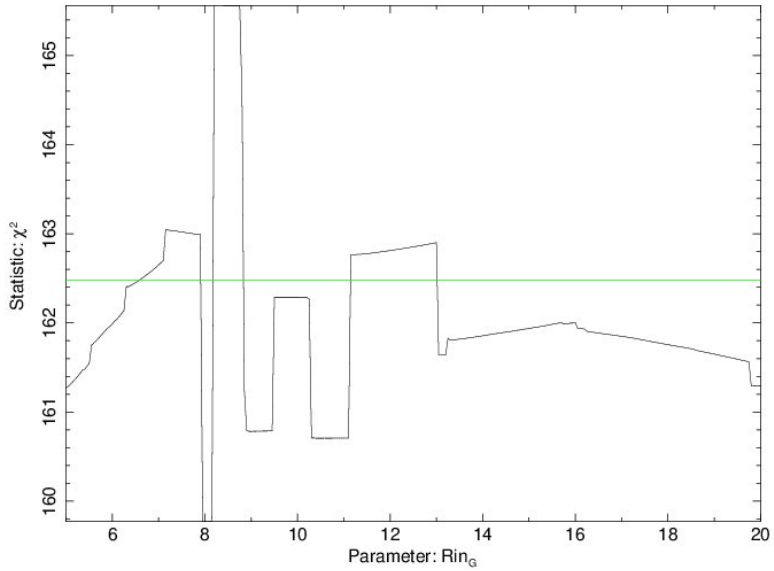

Figure 3.5: The dependence of χ^2 on the value of the inner radius of accretion disc after running `steppar` command between values 5-20 R_g in 301 steps. The green line marks the margin of region of 90 % confidence.

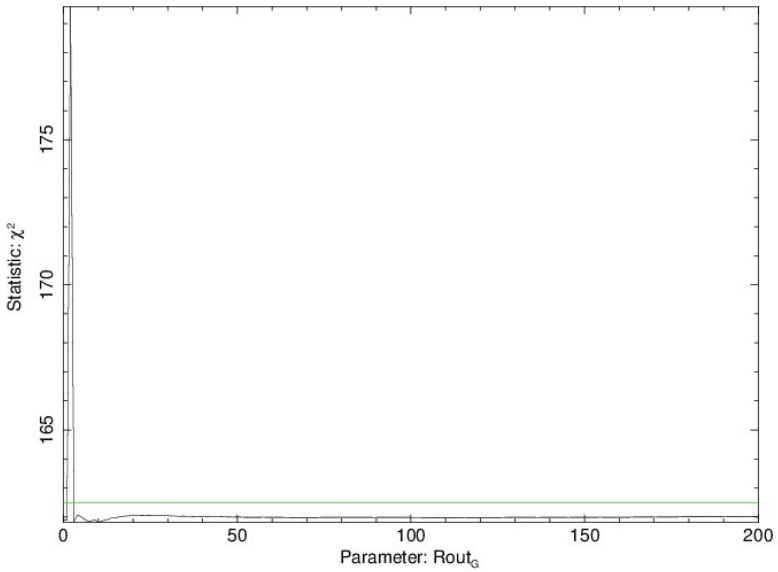

Figure 3.6: The dependence of χ^2 on the value of the outer radius of accretion disc after running `steppar` command between values 0-200 R_g in 201 steps. The green line marks the margin of region of 90 % confidence.

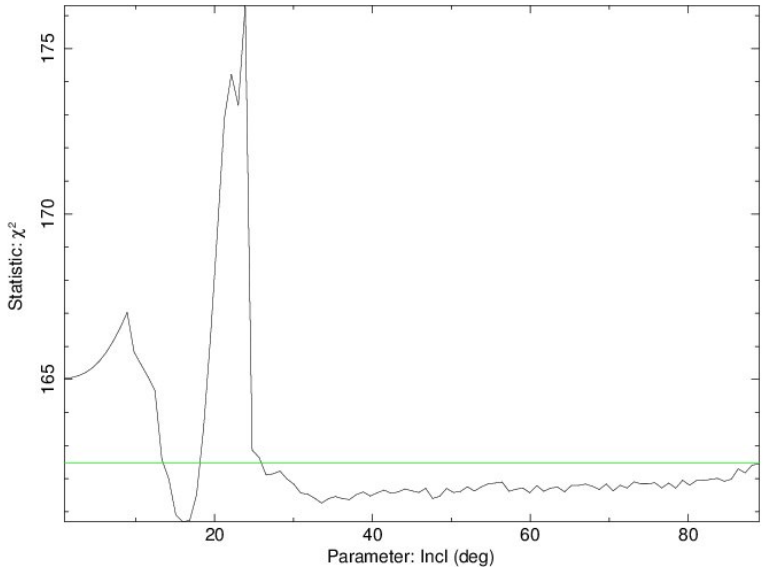

Figure 3.7: The dependence of χ^2 on the value of the inclination of source after running `steppar` command between values 1°-89° in 101 steps. The green line marks the margin of region of 90 % confidence.

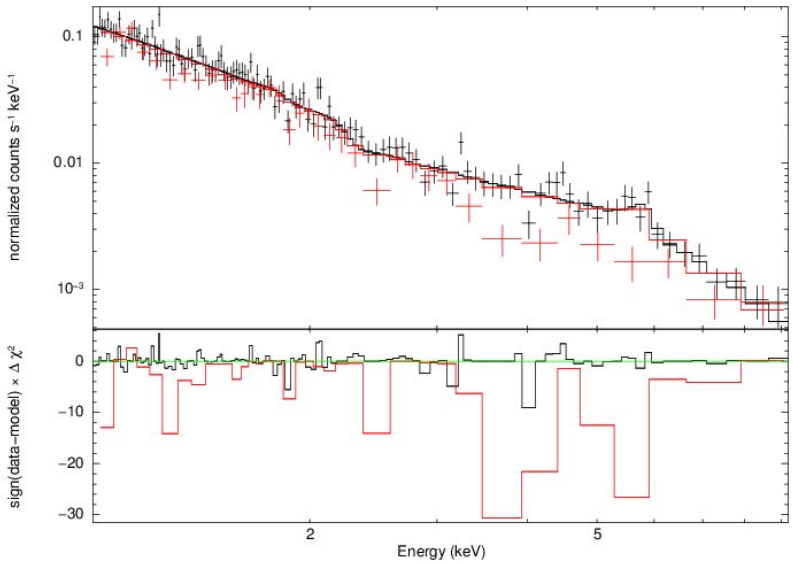

Figure 3.8: Up: PN spectra from XMM1 (black line) and XMM2 observation (red line). Bottom: Data residuals from the model fit, power-law model with extra Bremsstrahlung component and `laor` component (parameters are fixed to values, as proposed by Saxton et al. [2017] when using `kdblur` component).

The soft energy excess in XMM1 observation was modelled by Saxton et al. [2017] using model involving power-law component and reflection component convolved with `kdblur` component. We extended this analysis and first kept the value of the inner radius of accretion disc R_{in_G} fixed to 6 R_g, then we allowed all parameters to be fit, except for the emissivity index that was set to 3 in both cases. For the model with fixed value of the inner radius of accretion disc R_{in_G} to 6 R_g we obtained a fit with χ^2 of 410 for 393 d.o.f, whereas in case of all parameters being free we obtained a fit with χ^2 of 393 for 392 d.o.f. The results of proposed models along with their quality are reported in the Table 3.5.

We also checked the dependence of χ^2 on parameters of `kdblur` component (see Table 3.5) to see why the choice of letting them be free lead to improvement of fit goodness ($\Delta\chi^2$= 179 for 2 d.o.f. in case of the value of the inner radius of accretion disc R_{in_G} set to 6 R_g and $\Delta\chi^2$= 196 for 3 d.o.f. for all parameters being free). The Figures 3.9 and 3.10 shows that the values of the inner and outer radius of accretion disc R_{in_G} and R_{out_G} can be constrained. The situation is similar for the inclination of the radiation source, as depicted in the Figure 3.11. The F-test revealed that enabling the parameters to be fit is statistically significant with probability of 2.11×10^{-30} in case of the inner radius of accretion disc R_{in_G} set to 6 and 3.32×10^{-34} for all parameters free both with respect to the results obtained by using the fixed values of parameters.

The reflection of radiation - extra reflection component convolved with `kdblur` component - applied to both spectra of XMM1 and XMM2 observation and depicted in Figure 3.12 shows also no energy excess at low energies of XMM2 observation.

Table 3.5: Extension of free parameters in model involving extra reflection component convolved with `kdblur` component for XMM1 observation

Power-law		Reflection					χ^2_r
Γ	Norm $keV^{-1}cm^{-2}s^{-1}$	R_{in_G} R_g	R_{out_G} R_g	Inclination $^\circ$	ξ $erg\frac{cm}{s}$	Norm $\times 10^{-8}$	
1.78 ± 0.09	$9.31^{+1.03}_{-0.98} \times 10^{-5}$	fixed to 6	$6.39^{+0.15}_{-0.11}$	$9.7^{+4.4}_{-5.8}$	2000^{+160}_{-750}	$1.46^{+0.71}_{-0.16}$	$\frac{410}{393}$
$1.71^{+0.09}_{-0.10}$	$8.07^{+0.91}_{-1.34} \times 10^{-5}$	$2.94^{+0.61}_{-2.94}$	$4.0^{+1.6}_{-1.2}$	14^{+3}_{-7}	6200^{+1100}_{-3500}	$0.69^{+0.68}_{-0.21}$	$\frac{393}{392}$

All listed errors are 90 % confident.

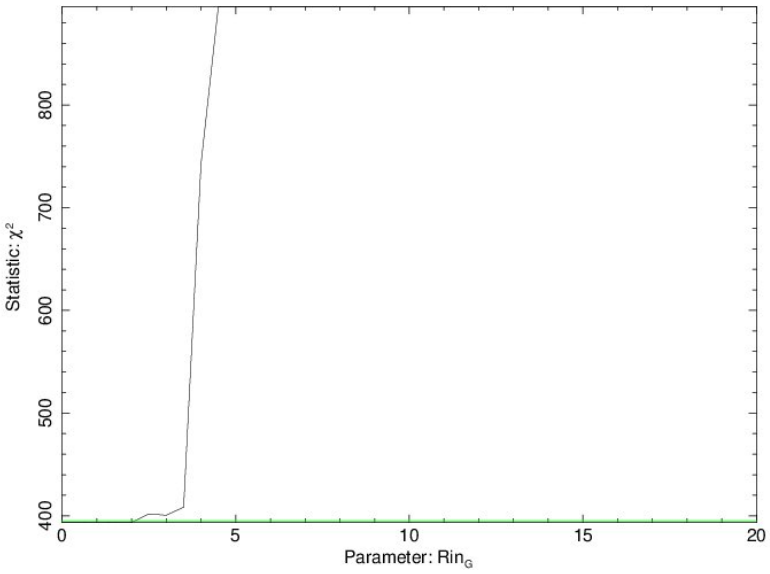

Figure 3.9: The dependence of χ^2 on the value of the inner radius of accretion disc after running `steppar` command between values 0-20 R_g in 41 steps. The green line marks the margin of region of 90 % confidence.

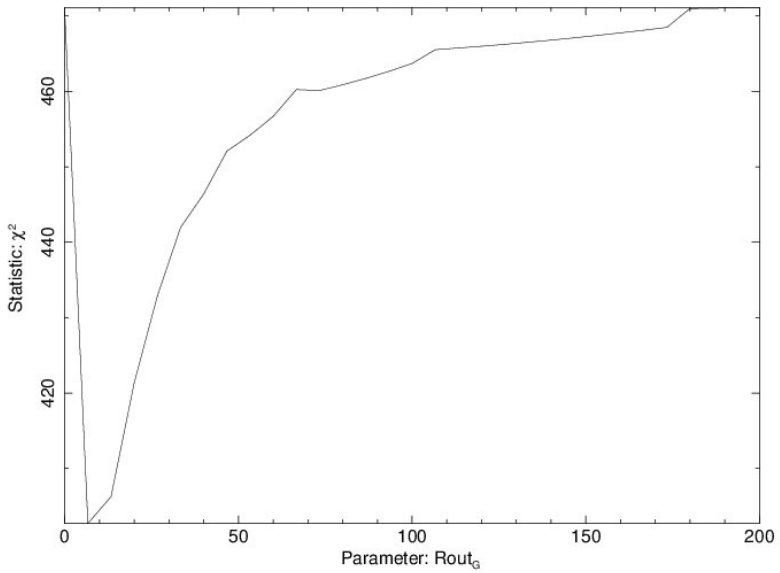

Figure 3.10: The dependence of χ^2 on the value of the outer radius of accretion disc after running `steppar` command between values 0-200 R_g in 31 steps. The green line marks the margin of region of 90 % confidence.

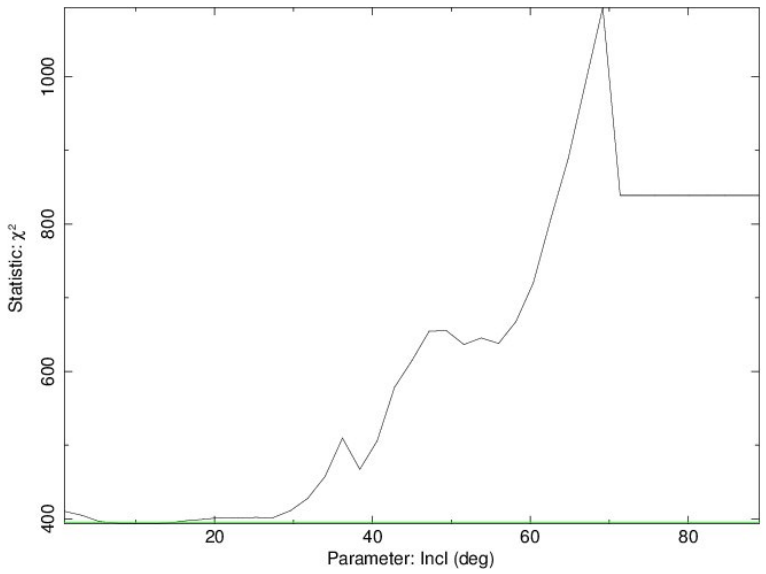

Figure 3.11: The dependence of χ^2 on the value of the inclination of source after running `steppar` command between values 1°-89° in 41 steps. The green line marks the margin of region of 90 % confidence.

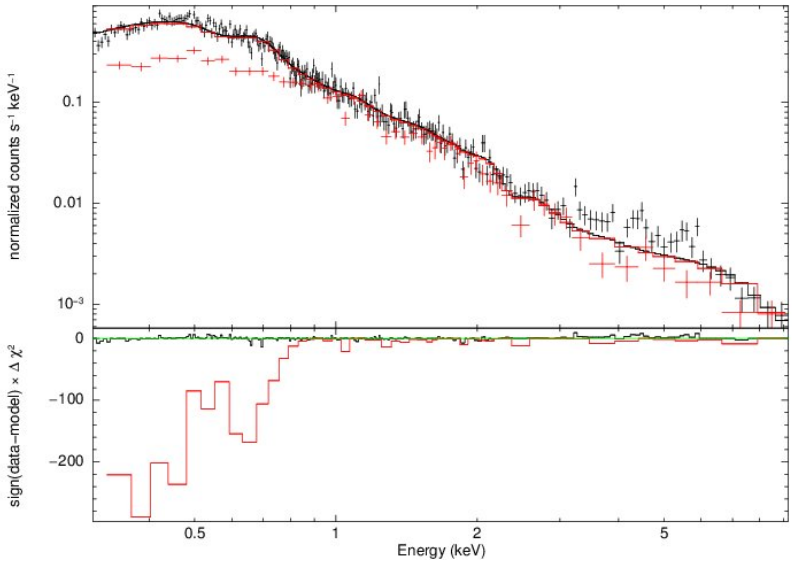

Figure 3.12: Up: PN spectra from XMM1 (black line) and XMM2 observation (red line). Bottom: Data residuals from the model fit, power-law model with extra reflection component convolved with `kdblur` component (parameters are fixed to values, as proposed by Saxton et al. [2017]).

4. Discussion and Conclusions

In this thesis we have studied the spectral characteristic of radiation emitted when a celestial object gets to sufficient distance from the galactic core to be torn apart by the gravitational pull of its SMBH. XMMSL1 J0740-85, first observed in 2014, is believed to be result of such a scenario and is therefore considered to be a TDE candidate. There are two interesting features of this particular TDE. The first is the thermal and non-thermal radiation profile, the second one are the residuals at the Fe Kα line energy band.

We have carried out the spectral re-analysis of two observations performed by the XMM-Newton telescope (separated approximately by 10 months). We have fit the data in the energy interval of 0.3 - 10.0 keV. The models we used to fit the X-ray spectra of both observations were all proposed by Saxton et al. [2017].

Our results are overall in good agreement with those published by Saxton et al. [2017] except for the fit goodness obtained for power-law model together with an extra reflection component convolved with `kdblur` component. In this case we got $\chi^2_{\rm r}$ of 589/395, whereas the fit goodness obtained by Saxton et al. [2017] is $\chi^2_{\rm r}$ of 664/396. The models we identified as best-fit candidates for XMM1 observation involve power-law component together with the black-body component and then with the Bremsstrahlung component. The fact that one of the best-fit models is involving black-body component could mean that there was a thermal component of the radiation present at that time. The XMM2 observation's best-fit candidates are double power-law and power-law alongside the Bremsstrahlung component. This result of spectral analysis suggests a possibility that the radiation did not have a thermal component anymore.

We subdued both XMM1 and XMM2 observation to more detailed spectral analysis in interval of 1 - 10 keV for studying the presence of Fe Kα line. In case of the XMM1 observation we proceeded in two ways. At first we fit the energy excess of XMM1 observation when adding `zgauss` component but the line emission we obtained did not correspond with Fe Kα line, however, the line width showed its broad profile with $\sigma = 0.30^{+0.64}_{-0.21}$ keV for extra black-body component and $\sigma = 0.30^{+0.63}_{-0.21}$ keV for extra Bremsstrahlung component. After that we pursued the fitting procedures while freezing the parameters of `laor` component to the values used by Saxton et al. [2017] when modelling the relativistic reflection using `kdblur` component. The results we obtained were characterised by fit goodness $\chi^2_{\rm r}$ of 163/188 for both extra black-body and Bremsstrahlung component. The fit goodness $\chi^2_{\rm r}$, when keeping the outer accretion disc radius $R_{\rm out\_G}$ fixed to 100, is 161/186 for both extra black-body and Bremsstrahlung component. Once we let all parameters free, except for the emissivity index, we obtained fit goodness $\chi^2_{\rm r}$ of 160/185 again for both extra black-body and Bremsstrahlung component. In case of the XMM2 observation we let all parameters of `laor` component be free and obtained fit goodness $\chi^2_{\rm r}$ of 68/61 for extra power-law component and $\chi^2_{\rm r}$ of 67/61 for extra Bremsstrahlung component.

We also extended the analysis of XMM1 observation based on the model proposed by Saxton et al. [2017] involving the simple power-law with reflection component convolved with `kdblur` component and let run the fitting procedures under two conditions. In the first variant we fixed the inner accretion disc radius $R_{\mathrm{in\_G}}$ to 6 and obtained a fit described by χ^2_{r} of 416/393. In the second case we let all parameters free and obtained the fit goodness χ^2_{r} of 393/392. If associated with marginally stable the first variant represents the result for a non-spinning SMBH,whereas the second one having the value of the inner accretion disc less than six ($\mathrm{R_{in\_G}} = 2.94^{+0.63}_{-2.94}\ \mathrm{R_g}$ precisely) stands for a SMBH with a non-zero spin value (Bardeen et al. [1972]). Both of these models fit the XMM1 observation data better than that proposed by Saxton et al. [2017] when keeping the parameters fixed.

According to the results there's a chance that the energy excess found in the spectrum of XMM1 observation could be caused by the presence of Fe Kα line in normal or highly ionised state. We also showed that neither the precise choice of fixed parameters of `laor` component, as proposed by Saxton et al. [2017], nor letting them be free, in case of both best-fit models does not have a huge impact on the fit goodness. However, working with free parameters we were able to obtain the emission line energies physically corresponding with that of Fe Kα line. The emission line energies found in the models for XMM2 observation are found at totally different energies meaning the Fe Kα line if present at all does not manifest itself at latter stages of this particular TDE or is simply shifted to region of lower energies. The results for XMM1 observation when applying the model involving `kdblur` component used to model the soft energy excess show that letting the parameters to be fit leads to better fit goodness. They also point out that in this case we can put constraints on the parameters in contrast to those of `laor` component. This could be caused due to the flux and errors in the energy bands, that the particular component focuses on. The lower energy band have a high flux and small errors enabling `kdblur` component to constrain its parameters. The parameters of `laor` component are on the other hand directed on the high energy band having smaller flux and bigger errors and are therefore not constrained.

The spectrum of XMM1 observation shows an energy excess at low energies caused by the relativistic reflection. The spectrum of XMM2 observation shows no signs of such energy excess. Both these results, the absence of Fe Kα line and no energy excess at low energies, could indicate that the reflective medium, e.g. accretion disc is getting thinner, i.e. it gets engulfed by the SMBH it is orbiting. They could also point out to the density drop of the accretion disc surface.

In case of having high-sensitivity X-ray data at disposal the `kyrline` component (Dovčiak et al. [2004b]) can be used to estimate the value of angular momentum of SMBH in non-active galactic centre as well as to put constraints on the size of accretion disc formed around it during the tidal disruption, both at the same time.

Bibliography

K. D. Alexander, E. Berger, J. Guillochon, B. A. Zauderer, and P. K. G. Williams. Discovery of an Outflow from Radio Observations of the Tidal Disruption Event ASASSN-14li. *The Astrophysical Journal Letters*, 819:L25, March 2016. doi: 10.3847/2041-8205/819/2/L25. URL `http://adsabs.harvard.edu/abs/2016ApJ...819L..25A`.

D. Alloin, R. Johnson, and P. Lira. *Physics of Active Galactic Nuclei at all Scales*. volume 693 of *Lecture Notes in Physics*. Springer, Berlin, Heidelberg, 2006. Active Galactic Nuclei: Basic Physics and Main Components, H. Netzer, p. 1-38.

I. Arcavi, A. Gal-Yam, M.a Sullivan, P. Yen-Chen, S. B. Cenko, and et al. A Continuum of H- to He-rich Tidal Disruption Candidates With a Preference for E+A Galaxies. *The Astrophysical Journal*, 793:38, September 2012. doi: 10.1088/0004-637X/793/1/38. URL `http://adsabs.harvard.edu/abs/2014ApJ...793...38A`.

K. Auchettl, J. Guillochon, and Ramirez-Ruiz Enrico. New physical insights about Tidal Disruption Events from a comprehensive observational inventory at X-ray wavelengths. *The Astrophysical Journal*, 838:149, April 2017. URL `http://adsabs.harvard.edu/abs/2016arXiv161102291A`.

J. M. Bardeen, W. H. Press, and S. A. Teukolsky. Rotating Black Holes: Locally Nonrotating Frames, Energy Extraction, and Scalar Synchrotron Radiation. *Astrophysical Journal*, 178:347–370, December 1972. doi: 10.1086/151796. URL `http://adsabs.harvard.edu/abs/1972ApJ...178..347B`.

J. S. Bloom, D. Giannios, B. D. Metzger, S. B. Cenko, D. A. Perley, N. R. Butler, N. R. Tanvir, A. J. Levan, P. T. O'Brien, L. E. Strubbe, F. De Colle, E. Ramirez-Ruiz, W. H. Lee, S. Nayakshin, Quataert E., A. R. King, A. Cucchiara, J. Guillochon, G. C. Bower, A. S. Fruchter, A. N. Morgan, and A. J. van der Horst. A Possible Relativistic Jetted Outburst from a Massive Black Hole Fed by a Tidally Disrupted Star. *Science*, 333:203, July 2011. doi: 10.1126/science.1207150. URL `http://adsabs.harvard.edu/abs/2011Sci...333..203B`.

W. N. Brandt, K. A. Pounds, and H. Fink. The unusual X-ray and optical properties of the ultrasoft active galactic nucleus Zwicky 159.034 (RE J1237+264). *Monthly Notices of the Royal Astronomical Society*, 273:L47–L52, April 1995. doi: 10.1093/mnras/273.1.L47. URL `http://adsabs.harvard.edu/abs/1995MNRAS.273L..47B`.

D. N. Burrows, J. A. Kennea, G. Ghisellini, V. Mangano, B. Zhang, K. L. Page, M. Eracleous, P. Romano, T. Sakamoto, A. D. Falcone, J. P. Osborne, S. Campana, A. P. Beardmore, A. A. Breeveld, M. M. Chester, R. Corbet, S. Covino, J. R. Cummings, P. D'Avanzo, V. D'Elia, P. Esposito, P. A. Evans, D. Fugazza, J. M. Gelbord, K. Hiroi, S. T. Holland, K. Y. Huang, M. Im, G. Israel, Y. Jeon, Y.-B. Jeon, H. D. Jun, N. Kawai, J. H. Kim, H. A. Krimm,

F. E. Marshall, P. Mészáros, H. Negoro, N. Omodei, W.-K. Park, J. S. Perkins, M. Sugizaki, H.-I. Sung, G. Tagliaferri, E. Troja, Y. Ueda, Y. Urata, R. Usui, L. A. Antonelli, S. D. Barthelmy, G. Cusumano, P. Giommi, A. Melandri, M. Perri, J. L. Racusin, B. Sbarufatti, M. H. Siegel, and N. Gehrels. Relativistic jet activity from the tidal disruption of a star by a massive black hole. *Nature*, 476:421–424, August 2011. doi: 10.1038/nature10374. URL `http://adsabs.harvard.edu/abs/2011Natur.476..421B`.

S. B. Cenko, H. A. Krimm, A. Horesh, A. Rau, D. A. Frail, J. A. Kennea, A. J. Levan, S. T. Holland, R. Butler, N, R. M. Quimby, J. S. Bloom, A. V. Filippenko, A. Gal-Yam, J. Greiner, S. R. Kulkarni, E. O. Ofek, F. Olivares E., P. Schady, J. M. Silverman, N. R. Tanvir, and D. Xu. Swift J2058.4+0516: Discovery of a Possible Second Relativistic Tidal Disruption Flare? *The Astrophysical Journal*, 753:77, July 2012. doi: 10.1088/0004-637X/753/1/77. URL `http://adsabs.harvard.edu/abs/2012ApJ...753...77C`.

M. Clavel, R. Terrier, A. Goldwurm, M. R. Morris, G. Ponti, S. Soldi, and G. Trap. Echoes of multiple outbursts of Sagittarius A revealed by Chandra. *Astronomy and Astrophysics*, 558, October 2013. doi: 10.1051/0004-6361/201321667. URL `http://adsabs.harvard.edu/abs/2013A%26A...558A..32C`.

J. R. Cummings, S. D. Barthelmy, A. P. Beardmore, D. N. Burrows, S. Campana, V. D'Elia, P. A. Evans, N. Gehrels, J. M. Gelbord, C. Guidorzi, S. T. Holland, E. A. Hoversten, J. A. Kennea, H. A. Krimm, O. M. Littlejohns, R. Margutti, F. E. Marshall, A. Melandri, C. Pagani, K. L. Page, D. M. Palmer, P. Romano, M. H. Siegel, E. Sonbas, R. L. C. Starling, G. Stratta, G. Tagliaferri, and E. Troja. GRB 110328A: Swift detection of a burst. *GCN, Circular Service*, 11823, March 2011. URL `http://adsabs.harvard.edu/abs/2011GCN..11823...1C`.

B. Czerny, D. Kunneriath, V. Karas, and T. K. Das. Multiple accretion events as a trigger for Sagittarius A* activity. *Astronomy and Astrophysics*, 555: A97, July 2013. doi: 10.1051/0004-6361/201118124. URL `http://adsabs.harvard.edu/abs/2013A%26A...555A..97C`.

J. L. Donley, W. N. Brandt, Michael Eracleous, and Th. Boller. Large-Amplitude X-Ray Outbursts from Galactic Nuclei: A Systematic Survey using ROSAT Archival Data. *The Astronomical Journal*, 124:1308–1321, September 2002. doi: 10.1086/342280. URL `http://adsabs.harvard.edu/abs/2002AJ....124.1308D`.

M. Dovčiak, S. Bianchi, M. Guainazzi, V. Karas, and G. Matt. Relativistic spectral features from X-ray-illuminated spots and the measure of the black hole mass in active galactic nuclei. *Monthly Notices of the Royal Astronomical Society*, 350:745–755, May 2004a. doi: 10.1111/j.1365-2966.2004.07683.x. URL `http://adsabs.harvard.edu/abs/2004MNRAS.350..745D`.

M. Dovčiak, V. Karas, and T. Yaqoob. An Extended Scheme for Fitting X-Ray Data with Accretion Disk Spectra in the Strong Gravity Regime. *The Astrophysical Journal Supplement Series*, 153:205–221, July 2004b. doi:

10.1086/421115. URL http://adsabs.harvard.edu/cgi-bin/nph-bib_query?bibcode=2004ApJS..153..205D&db_key=AST&data_type=HTML&format=&high=4230b2429422869.

A. C. Fabian, M. J. Rees, L. Stella, and N. E. White. X-ray fluorescence from the inner disc in Cygnus X-1. *Monthly Notices of the Royal Astronomical Society*, 238:729–736, May 1989. doi: 10.1093/mnras/238.3.729. URL http://adsabs.harvard.edu/abs/1989MNRAS.238..729F.

A. C. Fabian, D. R. Ballantyne, A. Merloni, S. Vaughan, K. Iwasawa, and Th. Boller. How the X-ray spectrum of a narrow-line Seyfert 1 galaxy may be reflection-dominated. *Monthly Notices of the Royal Astronomical Society*, 331: L35–L39, April 2002. doi: 10.1046/j.1365-8711.2002.05419.x. URL http://adsabs.harvard.edu/abs/2002MNRAS.331L..35F.

R. Genzel, C. Pichon, A. Eckart, O. E. Gerhard, and T. Ott. Stellar dynamics in the Galactic Centre: proper motions and anisotropy. *Monthly Notices of the Royal Astronomical Society*, 317:348–374, September 2000. doi: 10.1046/j.1365-8711.2000.03582.x. URL http://adsabs.harvard.edu/abs/2000MNRAS.317..348G.

S. Gezari, S. Basa, D. C. Martin, G. Bazin, K. Forster, B. Milliard, J. P. Halpern, P. G. Friedman, P. Morrissey, S. G. Neff, D. Schiminovich, M. Seibert, T. Small, and T. K. Wyder. UV/Optical Detections of Candidate Tidal Disruption Events by GALEX and CFHTLS. *The Astrophysical Journal*, 676:944–969, April 2008. doi: 10.1086/529008. URL http://adsabs.harvard.edu/abs/2008ApJ...676..944G.

S. Gillessen, R. Genzel, T. K. Fritz, E. Quataert, C. Alig, A. Burkert, J. Cuadra, F. Eisenhauer, O. Pfuhl, K. Dodds-Eden, C. F. Gammie, and T. Ott. A gas cloud on its way towards the supermassive black hole at the Galactic Centre. *Reviews of Modern Physics*, 481:51–54, January 2012. doi: 10.1038/nature10652. URL http://adsabs.harvard.edu/abs/2012Natur.481...51G.

J. G. Hills. Possible power source of Seyfert galaxies and QSOs. *Nature*, 254: 295–298, March 1975. doi: 10.1038/254295a0. URL http://adsabs.harvard.edu/abs/1975Natur.254..295H.

J. A. Irwin, R. N. Henriksen, M. Krause, Q. D. Wang, T. Wiegert, E. J. Murphy, G. Heald, and E. Perlman. CHANG-ES V: Nuclear Outflow in a Virgo Cluster Spiral after a Tidal Disruption Event. *The Astrophysical Journal*, 809:172, August 2015. doi: 10.1088/0004-637X/809/2/172. URL http://adsabs.harvard.edu/abs/2015ApJ...809..172.

E. Kara, J. M. Miller, Ch. Reynolds, and L. Dai. Relativistic reverberation in the accretion flow of a tidal disruption event. *Nature*, 535:388–390, July 2016. doi: 10.1038/nature18007. URL http://adsabs.harvard.edu/abs/2016Natur.535..388K.

D. Kazanas, K. Fukumura, E. Behar, I. Contopoulos, and Ch. Shrader. Toward a Unifed AGN Structure. *Astronomical Review*, 7:92–123, July 2012. doi: 10.1080/21672857.2012.11519707. URL http://adsabs.harvard.edu/abs/2012AstRv...7c..92K.

R. P. Kerr. Gravitational Field of a Spinning Mass as an Example of Algebraically Special Metrics. *Physical Review Letters*, 11:237–238, September 1963. doi: 10.1103/PhysRevLett.11.237. URL http://adsabs.harvard.edu/abs/1963PhRvL..11..237K.

Y. Kojima. The effects of black hole rotation on line profiles from accretion discs. *Monthly Notices of the Royal Astronomical Society*, 250:629–632, June 1991. doi: 10.1093/mnras/250.3.629. URL http://adsabs.harvard.edu/abs/1991MNRAS.250..629K.

S. Komossa. Ludwig Biermann Award Lecture: X-ray Evidence for Supermassive Black Holes at the Centers of Nearby, Non-Active Galaxies. *Reviews in Modern Astronomy*, 15, 2002. URL http://adsabs.harvard.edu/abs/2002RvMA...15...27K.

S. Komossa. Tidal disruption of stars by supermassive black holes: Status of observations. *, Journal of High Energy Astrophysics*, 7:148–157, September 2015. doi: 10.1016/j.jheap.2015.04.006. URL http://adsabs.harvard.edu/abs/2015JHEAp...7..148K.

S. Komossa and N. Bade. The giant X-ray outbursts in NGC 5905 and IC 3599:() hfill Follow-up observations and outburst scenarios. *Astronomy and Astrophysics*, 343, March 1999. URL http://adsabs.harvard.edu/abs/1999A%26A...343..775K.

A. Laor. Line profiles from a disk around a rotating black hole. *Astrophysical Journal*, 376:90–94, July 1991. doi: 10.1086/170257. URL http://adsabs.harvard.edu/abs/1991ApJ...376...90L.

Wei-Hua Lei, Q. Yuan, B. Zhang, and D. Wang. IGR J12580+0134: The First Tidal Disruption Event with an Off-beam Relativistic Jet. *The Astrophysical Journal*, 816:20, January 2016. doi: 10.3847/0004-637X/816/1/20. URL http://adsabs.harvard.edu/abs/2016ApJ...816...20L.

A. J. Levan, N. R. Tanvir, S. B. Cenko, D. A. Perley, K. Wiersema, J. S. Bloom, A. S. Fruchter, A. de Ugarte Postigo, P. T. O'Brien, N. Butler, A. J. van der Horst, G. Leloudas, A. N. Morgan, K. Misra, G. C. Bower, J. Farihi, R. L. Tunnicliffe, M. Modjaz, J. M. Silverman, J. Hjorth, C. Thöne, A. Cucchiara, J. M. Castro Cerón, A. J. Castro-Tirado, J. A. Arnold, M. Bremer, J. P. Brodie, T. Carroll, M. C. Cooper, P. A. Curran, R. M. Cutri, J. Ehle, D. Forbes, J. Fynbo, J. Gorosabel, J. Graham, D. I. Hoffman, S. Guziy, P. Jakobsson, A. Kamble, T. Kerr, M. M. Kasliwal, C. Kouveliotou, D. Kocevski, N. M. Law, P. E. Nugent, E. O. Ofek, D. Poznanski, R. M. Quimby, E. Rol, A. J. Romanowsky, R. Sánchez-Ramírez, S. Schulze, N. Singh, L. van Spaandonk, R. L. C. Starling, R. G. Strom, J. C. Tello, O. Vaduvescu, P. J. Wheatley, R. A. M. J. Wijers, J. M. Winters, and D. Xu. An Extremely Luminous

Panchromatic Outburst from the Nucleus of a Distant Galaxy. *Science*, 333: 199, July 2011. doi: 10.1126/science.1207143. URL http://adsabs.harvard.edu/abs/2011Sci...333..199L.

F. K. Liu, S. Li, and X. Chen. Interruption of Tidal-Disruption Flares by Supermassive Black Hole Binaries", journal = "The Astrophysical Journal Letters. 706:L133–L137, November 2009. doi: 10.1088/0004-637X/706/1/L133. URL http://adsabs.harvard.edu/abs/2009ApJ...706L.133L.

F. K. Liu, S. Li, and S. Komossa. A Milliparsec Supermassive Black Hole Binary Candidate in the Galaxy SDSS J120136.02+300305.5. *Astronomy and Astrophysics*, 786:103, May 2014. doi: 10.1088/0004-637X/786/2/103. URL http://adsabs.harvard.edu/abs/2014ApJ...786..103L.

J. Magorrian, S. Tremaine, D. Richstone, R. Bender, G. Bower, A. Dressler, S. M. Faber, K. Gebhardt, R. Green, C. Grillmair, J. Kormendy, and T. Lauer. The Demography of Massive Dark Objects in Galaxy Centers. *The Astronomical Journal*, 115:2285–2305, June 1998. doi: 10.1086/300353. URL http://adsabs.harvard.edu/abs/1998AJ....115.2285M.

B. D. Metzger, D. Giannios, and P. Mimica. Radio afterglow of the jetted tidal disruption event Swift J1644+57. *Journal of Physics: Conference Series*, 39: 04001, December 2012. doi: 10.1051/epjconf/20123904001. URL http://adsabs.harvard.edu/abs/2012EPJWC..3904001M.

J. Miralda-Escudé. The cloud of gas falling toward the central black hole in the milky way. *Tidal Disruption Events and AGN Outbursts*, 39:03003, December 2012. doi: 10.1051/epjconf/20123903003. URL http://adsabs.harvard.edu/abs/2012EPJWC..3903003M.

Ch. W. Misner, K. S. Thorne, and J. A. Wheeler. *Gravitation*. San Francisco: W. H. Freeman, p. 875-876, 1973. ISBN 0716703343.

M. Montesinos Armijo and José A. de Freitas Pacheco. Tidal Disruption Flares: The Accretion Disk Phase. *The Astronomical Journal*, 736:126, August 2011. doi: 10.1088/0004-637X/736/2/126. URL http://adsabs.harvard.edu/abs/2011ApJ...736..126M.

A. M. Read, M. Guainazzi, and S. Sembay. Cross-calibration of the XMM-Newton EPIC pn and MOS on-axis effective areas using 2XMM sources. *Astronomy and Astrophysics*, 564:A75, April 2014. doi: 10.1051/0004-6361/201423422. URL http://adsabs.harvard.edu/abs/2014A%26A...564A..75R.

M. J. Rees. Tidal disruption of stars by black holes of 10 to the 6th-10 to the 8th solar masses in nearby galaxies. *Nature*, 333:525–528, Juny 1988. doi: 10.1038/333523a0. URL http://adsabs.harvard.edu/abs/1988Natur.333..523R.

J. Reeves, Ch. Done, K. Pounds, Y. Terashima, K. Hayashida, N. Anabuki, M. Uchino, and Martin Turner. On why the iron K-shell absorption in AGN is not a signature of the local warm/hot intergalactic medium. *Monthly Notices of the Royal Astronomical Society*, 385:L108–L112, March 2008. doi:

10.1111/j.1745-3933.2008.00443.x. URL http://adsabs.harvard.edu/abs/2008MNRAS.385L.108R.

R. R. Ross and A. C. Fabian. A comprehensive range of X-ray ionized-reflection models. *Monthly Notices of the Royal Astronomical Society*, 358: 211–216, March 2005. doi: 10.1111/j.1365-2966.2005.08797.x. URL http://adsabs.harvard.edu/abs/2005MNRAS.358..211R.

R. D. Saxton, A. M. Read, P. Esquej, S. Komossa, S. Dougherty, P. Rodriguez-Pascual, and D. Barrado. A tidal disruption-like X-ray flare from the quiescent galaxy SDSS J120136.02+300305.5. *Astronomy and Astrophysics*, 541: A106, May 2012a. doi: 10.1051/0004-6361/201118367. URL http://adsabs.harvard.edu/abs/2012A%26A...541A.106S.

R. D. Saxton, A. M. Read, S. Komossa, and P. Esquej. A well-monitored, X-ray selected, tidal disruption event. *Tidal Disruption Events and AGN Outbursts*, 39:02002, December 2012b. doi: 10.1051/epjconf/20123902002. URL http://adsabs.harvard.edu/abs/2012EPJWC..3902002S.

R. D. Saxton, A. M. Read, S. Komossa, P. Lira, K. D. Alexander, and M. H. Wieringa. XMMSL1 J074008.2-853927: a tidal disruption event with thermal and non-thermal components. *Astronomy and Astrophysics*, 598:A29, January 2017. doi: 10.1051/0004-6361/201629015. URL http://adsabs.harvard.edu/abs/2017A%26A...598A..29S.

H. C. Spruit and D. A. Uzdensky. Magnetic Flux Captured by an Accretion Disk. *Astronomy and Astrophysics*, 629:960–968, August 2005. doi: 10.1086/431454. URL http://adsabs.harvard.edu/abs/2005ApJ...629..960S.

N. C. Stone. *The Tidal Disruption of Stars by Supermassive Black Holes An Analytic Approach*. Springer Theses, ISBN 978-3-319-12675-3, 2015. doi: 10.1007/978-3-319-12676-0. p. 1-12.

Y. Tanaka, K. Nandra, A. C. Fabian, H. Inoue, C. Otani, T. Dotani, K. Hayashida, K. Iwasawa, T. Kii, H. Kunieda, F. Makino, and M. Matsuoka. Gravitationally redshifted emission implying an accretion disk and massive black hole in the active galaxy MCG-6-30-15. *Nature*, 375:659–661, June 1995. doi: 10.1038/375659a0. URL http://adsabs.harvard.edu/abs/1995Natur.375..659T.

T.M. Tauris and E.P.J. van den Heuvel. *Chapter 16: Formation and evolution of compact stellar X-ray sources*. Compact stellar X-ray sources. Edited by Walter Lewin and Michiel van der Klis. Cambridge Astrophysics Series, No. 39. Cambridge, UK: Cambridge University Press, ISBN 978-0-521-82659-4„ 2006. doi: 10.2277/0521826594. p. 623 - 665.

S. Umbreit. Astrophysics: Two black holes found in a star cluster. *Nature*, 490: 46–47, October 2012. doi: 10.1038/490046a. URL http://adsabs.harvard.edu/abs/2012Natur.490...46U. F. MIRABEL (CEA AND INST. ASTRON. SPACE PHYS.)/CONICET ARGENTINA/ESA/NASA.

Sjoert van Velzen and Glennys R. Farrar. Measurement of the Rate of Stellar Tidal Disruption Flares. *The Astrophysical Journal*, 792:53, September 2014. doi: 10.1088/0004-637X/792/1/53. URL http://adsabs.harvard.edu/abs/2014ApJ...792...53V.

N. Vlahakis and A. Königl. Magnetic Driving of Relativistic Outflows in Active Galactic Nuclei. I. Interpretation of Parsec-Scale Accelerations. *The Astrophysical Journal,*, 605:656–661, April 2004. doi: 10.1086/382670. URL http://adsabs.harvard.edu/abs/2004ApJ...605..656V.

J. Wilms, A. Allen, and R. McCray. On the Absorption of X-Rays in the Interstellar Medium. *The Astrophysical Journal*, 542:914–924, October 2000. doi: 10.1086/317016. URL http://adsabs.harvard.edu/abs/2000ApJ...542..914W.

M. Zajaček, V. Karas, and A. Eckart. Dust-enshrouded star near supermassive black hole: predictions for high-eccentricity passages near low-luminosity galactic nuclei. *Astronomy and Astrophysics*, 565:A17, May 2014. doi: 10.1051/0004-6361/201322713. URL http://adsabs.harvard.edu/abs/2014A%26A...565A..17Z.

W. Zhang, W. Yu, V. Karas, and M. Dovčiak. Predictions for the Reverberating Spectral Line from a Newly Formed Black Hole Accretion Disk: Case of Tidal Disruption Flares. *The Astrophysical Journal*, 807:89, July 2015. doi: 10.1088/0004-637X/807/1/89. URL http://adsabs.harvard.edu/abs/2015ApJ...807...89Z.

List of Figures

List of Tables

List of Abbreviations

AGN - Active Galactic Nucleus

ASAS-SN - All Sky Automated Survey for Supernovae

BH - Black Hole

EPIC - European Photon Imaging Camera

GALEX - Galaxy Evolution Explorer

INTEGRAL - International Gamma-Ray Astrophysics Laboratory

SAS - Standard Analysis System

SDSS - Sloan Digital Sky Survey

SMBH - Super-massive Black Hole

SMBHB - Super-massive Black Hole Binaries

ROSAT - Röntgen Satellite

TDE - Tidal Disruption Event

UV - Ultraviolet

XSPEC - X-ray Spectra Fitting Package